Check for updates

Received: 3 March 2023 | Revised: 3 December 2023 | Accepted: 10 December 2023

DOI: 10.1002/glia.24498

GLIA

WILEY

RESEARCH ARTICLE

Ascorbic acid and its transporter SVCT2, affect radial glia cells differentiation in postnatal stages

Natalia Saldivia[1] | Katterine Salazar[1] | Manuel Cifuentes[2] | Francisca Espinoza[1] | Fiona E. Harrison[3] | Francisco Nualart[1]

[1]Laboratory of Neurobiology and Stem Cells, NeuroCellT, Department of Cellular Biology, Center for Advanced Microscopy, CMA BIO BIO, Faculty of Biological Sciences, Universidad de Concepción, Concepción, Chile

[2]Department of Cell Biology, Genetics and Physiology, Universidad de Málaga, IBIMA, Málaga, Spain

[3]Division of Diabetes, Endocrinology and Metabolism, Department of Medicine, Vanderbilt University Medical Center, Nashville, USA

Correspondence
Francisco Nualart and Katterine Salazar, Laboratory of Neurobiology and Stem Cells, NeuroCellT, Department of Cellular Biology, Center for Advanced Microscopy, CMA BIO BIO, Faculty of Biological Sciences, Universidad de Concepción, Chile.
Email: frnualart@udec.cl and katt.salazar@gmail.com

Manuel Cifuentes, Department of Cell Biology, Genetics and Physiology, Universidad de Málaga, IBIMA, Málaga, Spain.
Email: mcifuentes@uma.es

Present addresses
Natalia Saldivia, Department of Anatomy and Cell Biology, University of Illinois at Chicago, Chicago, Illinois, USA; and Francisca Espinoza, Neurodevelopmental Biology Unit, Biomedical Sciences Research Laboratory, Department of Basic Science, Faculty of Medicine, Universidad Católica de la Santísima Concepción, Concepción, Chile.

Funding information
Agencia Nacional de Investigación y Desarrollo (ANID) - Programa de Investigación Asociativa (PIA) Chile, Grant/Award Number: ECM12; Fondo Nacional de Desarrollo Científico y Tecnológico, Grant/Award Numbers: 1190848, 1221147

Abstract

Radial glia (RG) cells generate neurons and glial cells that make up the cerebral cortex. Both in rodents and humans, these stem cells remain for a specific time after birth, named late radial glia (lRG). The knowledge of lRG and molecules that may be involved in their differentiation is based on very limited data. We analyzed whether ascorbic acid (AA) and its transporter SVCT2, are involved in lRG cells differentiation. We demonstrated that lRG cells are highly present between the first and fourth postnatal days. Anatomical characterization of lRG cells, revealed that lRG cells maintained their bipolar morphology and stem-like character. When lRG cells were labeled with adenovirus-eGFP at 1 postnatal day, we detected that some cells display an obvious migratory neuronal phenotype, suggesting that lRG cells continue generating neurons postnatally. Moreover, we demonstrated that SVCT2 was apically polarized in lRG cells. In vitro studies using the transgenic mice $SVCT2^{+/-}$ and $SVCT2^{tg}$ (SVCT2-overexpressing mouse), showed that decreased SVCT2 levels led to accelerated differentiation into astrocytes, whereas both AA treatment and elevated SVCT2 expression maintain the lRG cells in an undifferentiated state. In vivo overexpression of SVCT2 in lRG cells generated cells with a rounded morphology that were migratory and positive for proliferation and neuronal markers. We also examined mediators that can be involved in AA/SVCT2-modulated signaling pathways, determining that GSK3-β through AKT, mTORC2, and PDK1 is active in brains with high levels of SVCT2/AA. Our data provide new insights into the role of AA and SVCT2 in late RG cells.

KEYWORDS
ascorbic acid, cerebral cortex, late radial glia, neuronal differentiation, SVCT2, vitamin C

This is an open access article under the terms of the Creative Commons Attribution-NonCommercial License, which permits use, distribution and reproduction in any medium, provided the original work is properly cited and is not used for commercial purposes.
© 2024 The Authors. GLIA published by Wiley Periodicals LLC.

1 | INTRODUCTION

The embryonic or early RG cells generate, directly or through intermediate progenitors (IP), the vast amount of neuronal and glial cells in the cerebral cortex (Kriegstein & Alvarez-Buylla, 2009; Mori et al., 2005; Pebworth et al., 2021). This cell type displays a bipolar morphology, radially extending two thin processes away from the cell body and a nucleus that moves between the ventricular (VZ) and subventricular zones (SVZ) of the lateral ventricles, due to interkinetic nuclear migration (Noctor et al., 2002; Villalba et al., 2021). One of the processes of RG is a long basal process that reaches the outer pial surface through an end foot, serves as a scaffold for neuroblast migration (Kosodo & Huttner, 2009; Kriegstein & Alvarez-Buylla, 2009), and receives signals that modulate its differentiation such as retinoic acid, a powerful inducer of neuronal differentiation released from meninges (Glaser & Brustle, 2005; Jones-Villeneuve et al., 1983; Siegenthaler et al., 2009). In addition, RG cells have a short apical process that exhibits a primary cilium, allowing embryonic RG cells to contact the cerebrospinal fluid (CSF) (Spear & Erickson, 2012; Tong et al., 2014; Villalba et al., 2021). Interestingly, after birth, embryonic RG cells persist in the VZ and SVZ of the lateral ventricle, for up to 15 days in rodents and approximately up to 3 months in human brains, named late or postnatal RG (lRG) (Merkle et al., 2004; Sanai et al., 2011; Tramontin et al., 2003; Voigt, 1989). After this postnatal period, RG disappears, and a subpopulation of these cells transitions into adult NSCs (type B cells), giving rise to interneurons (Fuentealba et al., 2015; Furutachi et al., 2015; Ortiz-Alvarez & Spassky, 2021; Redmond et al., 2019). There is a clear biological importance of the presence of postnatal neural stem cells which could be a potential therapeutic target for neurological lesions that affect newborns, yet little attention has been given to the lRG cells. Therefore, we performed a systematic characterization of lRG cells and investigated whether molecules that are highly concentrated in the CSF, such as AA (Spector & Lorenzo, 1974), could be involved in lRG cell differentiation.

At physiological pH, vitamin C is mainly found in its reduced state, as AA (Nualart et al., 2014; Rice, 2000). In the brain, AA is transported by the sodium-dependent vitamin C transporter 2 (SVCT2) (Harrison & May, 2009; Nualart et al., 2014; Tsukaguchi et al., 1999). Studies with transgenic mice highlight the importance of SVCT2 in AA transport; AA levels were undetectable and significantly decrease in SVCT2$^{-/-}$ and SVCT2$^{+/-}$ mice, respectively (Meredith et al., 2011; Sotiriou et al., 2002). Furthermore, transgenic mice overexpressing SVCT2 (SVCT2^{tg}), have significantly elevated AA levels in the brain (Harrison et al., 2012). Besides the well-known function of AA as an antioxidant and free radical scavenger (Bodannes & Chan, 1979), this vitamin has multiple other specific functions in the brain (Ferrada et al., 2020; Ferrada et al., 2021; Harrison & May, 2009; Nualart et al., 2014). SVCT2 has also been detected in multiple types of brain cells (Astuya et al., 2005; Garcia Mde et al., 2005; Mun et al., 2006; Nualart et al., 2012; Portugal et al., 2017; Salazar et al., 2014; Salazar et al., 2017; Ulloa et al., 2013; Ulloa et al., 2019). Ongoing investigations have shown that AA incorporation by SVCT2 could be important for neuronal maturation (Espinoza et al., 2020; Salazar et al., 2016; Salazar et al., 2021). Moreover, in neural stem cells, AA and SVCT2 promoted neuronal differentiation (Lee et al., 2003; Oyarce et al., 2018; Pastor et al., 2013). Interestingly, during mouse cerebral cortex development, SVCT2 ventricular polarization was detected in embryonic RG cells (Silva-Alvarez et al., 2016). In addition, analysis in human brains showed that SVCT2 is localized in the inner and outer SVZ (Silva-Alvarez et al., 2016). These data suggest that embryonic RG would take up AA from the CSF. On note, in vitro analysis of embryonic RG cells primary cultures showed that AA stimulates radial morphology while maintaining their undifferentiated phenotype (Silva-Alvarez et al., 2016). In line with this notion, several studies have proposed AA as a molecule that maintains an undifferentiated state, both in stem cells and in cell reprogramming (Esteban et al., 2010; Gao et al., 2013; Stadtfeld et al., 2012; Wang et al., 2011; Wu et al., 2014).

In this study, we found a high presence of lRG cells in the cortex of rodents during the first and fourth postnatal days. Furthermore, we detected SVCT2 ventricularly polarized in lRG cells, an expression that decreases as postnatal development proceeds. Our in vitro analysis of enriched primary lRG-like cells cultures using SVCT2^{tg} mice demonstrated that high levels of SVCT2 as well as AA treatment enhance the radial phenotype of lRG-like cells, maintaining their undifferentiated phenotype. In contrast, primary cultures obtained from SVCT2$^{+/-}$ showed that low levels of SVCT2 led to an astrocytic differentiation. Finally, one of the most remarkable results was to find out that in vivo overexpression of SVCT2 in lRG cells generates cells with rounded morphology that co-localized with neuronal markers, suggesting that SVCT2 and AA play a role in the differentiation of lRG cells.

2 | METHODS

2.1 | Animals

Experimental animals, Sprague Dawley rats, were managed according to the "Manual de Normas de Bioseguridad" (Comisión Nacional de Ciencia y Tecnología, CONICYT) and the Animal Care and Use Committee of the Universidad de Concepción (Concepción, Chile). The experimental protocols were approved by the Universidad de Concepción Licensing Committee, grant number 1181243. The studies presented in this paper were performed in rats. As SVCT2 transgenic rats do not exist, SVCT2 transgenic mice (SVCT2^{tg}, SVCT2$^{+/-}$, SVCT2-*wild type*) were used for primary cultures and functional assays. The use of transgenic mouse models was approved by the Vanderbilt University Institutional Committee for Animal Use and Care and was conducted in accordance with NIH guidelines. All the animals were housed under a 12 h light/dark cycle with food and water available ad libitum.

2.2 | Primary culture

Cells were obtained from 1-day-old Sprague Dawley rats or SVCT2^{tg}, SVCT2$^{+/-}$ and SVCT2-*wild type* mice. Dissection of the brain was performed, the meninges removed, and the tissue was digested using

10981136, 0, Downloaded from https://onlinelibrary.wiley.com/doi/10.1002/glia.24498 by Chun-Consorcio De Bibliotecas, Wiley Online Library on [26/01/2024]. See the Terms and Conditions (https://onlinelibrary.wiley.com/terms-and-conditions) on Wiley Online Library for rules of use; OA articles are governed by the applicable Creative Commons License

trypsin and 0.2% (w/v) EDTA in 0.1 M phosphate buffer (pH 7.4, 320 mOsm) and mechanically disaggregated in MEM medium (GIBCO). The cells were seeded at a density of 6×10^5 cells/cm^2 on poly-L-lysine-coated dishes (0.1 mg/mL poly-L-lysine; Sigma-Aldrich, St. Louis, MO, USA) and cultured with BME medium (GIBCO) supplemented with 0.1% w/v glucose, 10% FBS, 2 mM L-glutamine and 100 U/mL penicillin–streptomycin (GIBCO) and 2.5 μg/mL fungizone (Thermo Fisher Scientific). The cultures were maintained in an incubator at 37°C, 5% CO_2, and 95% humidity. Some 1-day in vitro cultures were treated with 200 μM L-AA (Sigma-Aldrich, St. Louis, MO, USA) or phosphate-buffered saline (PBS) every 24 h for 7 days.

2.3 | Immunocytochemistry

Cells were seeded on coverslips and fixed with 4% paraformaldehyde (PFA) in PBS for 30 min at room temperature. Subsequently, the cells were washed with tris-phosphate buffer (pH 7.8) with 0.2% v/v triton X-100 (Sigma) and incubated with the following antibodies: goat anti-SVCT2 (1:50, G19 Santa Cruz Biotechnology, Santa Cruz, CA, USA); chicken anti-vimentin (1:400, #AB5733, Millipore, Temecula, CA, USA,), rabbit anti-3-phospho-glycerol dehydrogenase (3PGDH; 1:300, kindly donated by Dr. Shigeki Furuya), rabbit anti-glial fibrillary acidic protein (GFAP,1:200, #Z0334, DAKO, Carpinteria, CA, USA), anti-Sox2 (1:200, ab97959, Abcam, Cambridge, United Kingdom), mouse anti-nestin (1:50, MAB353, EMD Millipore, USA biosciences, Franklin Lakes, NJ, USA) in the same buffer containing 1% bovine serum albumin (BSA) overnight at 22°C. Cells were washed with tris-phosphate buffer and incubated for 2 h with affinity-purified secondary antibodies conjugated to cyanine dyes (Cy2, Cy3 or Cy5, 1:200; Jackson Immuno Research, West Grove, PA, USA). Höechst 33,342 (1:1000, Molecular Probes, Eugene, Oregon, USA) was used for nuclear staining. Multi-labeled images were obtained by confocal microscopy (LSM 780, Carl Zeiss). In addition, this confocal microscope has a multiphoton pulsed laser adjustable from 680 to 1080 nm, in steps of 1 nm, which was used as a tool to obtain images through two-photon microscopy. Two-dimensional reconstructions in the xz and yz planes and three-dimensional projections were performed with the Zen 2011 V7.0.7.2 software (Zeiss).

2.4 | Laser microdissection and RT-PCR

Rat brains were initially fixed by vascular perfusion and then by immersion with methacarn (methanol 60% v/v, chloroform 30% v/v, and glacial acetic acid 10% v/v). After fixation, 60-80 μm sections were made with a vibratome (Vibratome line, Leica VT 10005). These slices were mounted on PEN (polyethylene naphtholate) membrane-framed slides for subsequent microdissection of VZ-SVZ of lateral ventricles and cerebral cortex using a laser microdissection microscope system (LMD 7000, Leica) with a UV laser. RNA extraction was performed by column using the RNAqueous®-Micro Total RNA Isolation Kit (ThermoFisher Scientific). cDNA reaction was performed using RevertAid® H Minus M-MuLV reverse transcriptase enzyme (Perkin Elmer, Waltham, MA, USA). Negative controls were performed using the same protocol described but without the addition of reverse transcriptase enzyme.

2.5 | Quantitative RT-PCR (qRT-PCR) analyses

qRT-PCR reaction was performed with Brilliant II SYBR Green qPCR Master Mix kit (#600828, Agilent Technologies, Santa Clara, CA, USA), using the Mastercycler epgradient realplex2 (Eppendorf). Initially, calibration and efficiency curves were performed using serial dilutions. Each primer set was: SVCT2 forward: 5′-TGCCAGGAAGGGTGTACTTC-3′, reverse 5′-CCGGTACCAAATATGCCATC-3′, GLUT1: forward 5′-AGCAGTGSSGTC-CAGGAGGA-3′; reverse: 5′-CTGGTCTCAGGCAAGGGAAG-3′, cyclophilin forward: 5′-TGGAGATGAATCTGTAGGAGGAG-3′ and reverse: 5′-TAC-CACATCCATGCCCTCTAGAA-3′. Each reaction mixture was performed in triplicate and quantification of mRNA for SVCT2 and GLUT1 was performed relative to the reference gene cyclophilin. Relative expression was calculated and plotted from the $2^{-\Delta\Delta Ct}$ method.

2.6 | In situ hybridization

A cDNA of 620 base pair sequence of rat SVCT2 was cloned into the pCR®4Blunt-TOPO® (Clontech, Palo Alto, CA, USA) and used to generate sense and antisense probes tagged with digoxigenin-uridine triphosphate by in vitro transcription with T3 or T7 RNA polymerase following the manufacturer's procedure (Roche, Mannheim, Germany). In situ hybridization was performed on formalin fixed, paraffin embedded post-natal brain cortex sections mounted on Vectabond® (Vector Laboratories, Inc., CA, USA) glass slides. The samples were deparaffinized in HistoClear (National Diagnostics) and rehydrated with decreasing concentrations of graded ethanol. Then, samples were treated with proteinase K (1 μg/μL; Sigma) and fixed with 4% PFA. The tissues were acetylated and incubated in pre-hybridization solution (280 mM NaCl; 1 mM Tris-Base; 9 mM Tris–HCl; 3.4 mM NaH_2PO_4; 5 mM Na_2HPO_4), 1 μL of tRNA (100 mg/mL) (Roche Applied Science), 50% v/v formamide, 10 mM DTT, 10% w/v dextran sulfate, 1X Denhart solution (0.2% v/v ficoll, 0.2% v/v polyvinylpyrrolidone) and 0.2% w/v BSA. The hybridization solution which was prepared by incubating the anti-sense and sense probes. The slides were incubated at 42°C overnight. Then, astringent washes were performed with citrate saline solution (SSC, 3 M NaCl, 0.3 M sodium citrate, pH 7.0). Subsequently, samples were incubated in 2% v/v normal sheep serum (SON). Visualization of digoxigenin was performed by incubation with the anti-digoxigenin alkaline phosphatase-conjugated antibody. To proceed to in situ hybridization development, samples were washed with Tris–HCl pH 9.5. To reveal alkaline phosphatase activity, the slices were incubated in the dark with NBT/BCIP in distilled water (NTB/BCIP tablets, Roche Applied Science). The samples were observed and imaged under brightfield microscopy using a Leica DME microscope (Leica microsystem Inc.).

10981136, 0, Downloaded from https://onlinelibrary.wiley.com/doi/10.1002/glia.24498 by Cbua-Consorcio De Bibliotecas, Wiley Online Library on [26/01/2024]. See the Terms and Conditions (https://onlinelibrary.wiley.com/terms-and-conditions) on Wiley Online Library for rules of use; OA articles are governed by the applicable Creative Commons License

2.7 | Immunohistochemistry

Animals were perfused transcardially with 0.9% saline followed by 4% PFA, brains were dissected and post-fixed in the same fixative overnight at 4°C. 40 μm-thick frontal sections were sequentially cut using a vibratome. In all immunohistochemistry, 40 μm-thick slices were used, unless otherwise specified. For 7 μm brain slices, brains were washed in increasing concentrations of alcohol, then was transferred to the HistoClear and embedded in paraffin. 7-μm-thick frontal sections were sequentially cut using a microtome (Leica Reichert-Jung 2040 Autocut Microtome). Other primary antibodies used in addition to those mentioned above were: mouse anti-βIII-tubulin (Tuj1; 1:1000; Promega, Madison, Wisconsin, USA), rabbit anti-GLUT1 (1:100, #07-1401, EMD Millipore, USA), guinea pig anti-doublecortin (DCX, 1:200, AB2253, EMD Millipore, USA), mouse anti-NeuN (1:500, MAB377, EMD Millipore, USA) and anti-chicken Tbr2 (1:200, AB15894 EMD Millipore, USA). Then, samples were washed with tris-phosphate buffer and incubated for 2 h with affinity-purified secondary antibodies conjugated to cyanine dyes and Höechst 33,342. Multi-labeled images were obtained by confocal microscopy (LSM 780, Carl Zeiss).

2.8 | Transmission electron microscopy and immunogold staining

For immunogold electron microscopy (TEM-IG), pre-embedding immunogold staining was performed as previously described (Baeza et al., 2021; Martinez et al., 2019). Briefly, animals were deeply anesthetized and perfused transcardially with 0.9% saline, followed by 2% PFA/2.5% glutaraldehyde in PBS. Brains were dissected and post-fixed with 2% PFA at 4°C overnight and cut into 50 μm semi-thin sections using a vibratome. The sections were first incubated with anti-SVCT2 or anti-GFAP antibodies (1:100, z0334, DAKO) at 4°C for 4 days, and further incubated with secondary donkey anti-rabbit IgG or Donkey anti-Goat IgG diluted conjugated to colloidal ultrasmall gold particles (EMS-#25801) at a 1:50 dilution for 24 h at 4°C. After enhancement of gold particles with silver, sections were washed, postfixed with 2.5% glutaraldehyde, and postfixed with 1% osmium tetroxide. The antibodies were diluted in blocking buffer (0.5% BSA, 0.1% Fish Gelatin in 0.1 M phosphate buffer, pH 7.4). The tissue sections were dehydrated and embedded in Araldite 502 (EMS). Finally, 60 nm cuts were made on the UltraCutE ultramicrotome (Reichert-Jung. Germany) with a diamond blade and collected on 200 mesh copper grids for observation under a transmission electron microscope (Jeol Jem-1400).

2.9 | In vivo transduction

To label lRG cells in vivo, adenoviruses were generated as previously described (Baeza et al., 2021). The adenovirus contains a sequence, under the H1 promoter, of unrelated shRNA to inhibit the *E. coli* β-galactosidase enzyme and as a reporter gene, under the human ubiquitin promoter, the green fluorescent protein (eGFP). In all experiments, 1-day postnatal rats were placed in latex glove and immerse up to the neck in crushed ice for 3 min and a single injection of 2 μL (1μg/μl) of adenovirus was performed. For this purpose, an imaginary line was drawn between the eye and the bregma and at 1.0 mm caudal to the midpoint of this line and a 2.0 mm deep brain injection was performed. After the pup recovered its body temperature, it was returned to its litter. The animals were kept for different periods of time, during which they were monitored to detect pain and distress. After the required maintenance time, the rats were sacrificed for immunohistochemical and/or confocal microscopy analysis.

2.10 | In vivo electroporation

DNA constructs containing the human SVCT2 transporter gene fused to the yellow fluorescent protein (hSVCT2-EYFP) and as a control, the same construct expressing only the reporter gene (EYFP-N1) (Clontech) was used (Salazar et al., 2016). Since all electroporation will be shown in green, the nomenclature for these plasmids will be written as eGFP. These plasmids were amplified by the transformation of chemically competent One Shot® TOP10 Escherichia Coli bacteria (Invitrogen) and subsequently, purification was performed using the endotoxin-free plasmid purification kit (Macherey-Nagel) according to the protocol specified by the manufacturer. The intraventricular injection was similarly performed as explained above (in vivo transduction) and immediately after the plasmid injection, using a square pulse electroporator (BTX 830), five pulses of 100 V for 10 ms each were applied. After the rats recovered their normal body temperature, they were returned to their litter.

2.11 | In vivo BrdU labeling

One intraventricular injection was performed in 1-day postnatal rats using 5-bromo-2′-deoxyuridine (BrdU, Sigma). An injection of 3 μL of BrdU (50 mg/kg) diluted in sterile saline was performed. After 2 days, the animals were fixed with 4% PFA, the brains were removed and cut with a vibratome. For BrdU detection, before performing immunohistochemistry, an additional step was carried out to denature the DNA using 1 M HCl at 45°C for 30 min. The acid was neutralized by washing with tris-phosphate buffer and then immunohistochemistry was performed using anti-BrdU antibody (1:500, Abcam, AB1893).

2.12 | Ascorbic acid content

Hindbrain was removed at the same time as the cortex and frozen at −80°C until used for determination of AA. Tissues were weighed and homogenized by hand in Sodium EDTA with 25% metaphosphoric acid and diluted in deionized water before being assayed by HPLC with electrochemical detection as described previously (Dixit et al., 2017).

10981136, 0, Downloaded from https://onlinelibrary.wiley.com/doi/10.1002/glia.24498 by Chuo-Consorcio De Bibliotecas, Wiley Online Library on [26/01/2024]. See the Terms and Conditions (https://onlinelibrary.wiley.com/terms-and-conditions) on Wiley Online Library for rules of use; OA articles are governed by the applicable Creative Commons License

2.13 | Western blotting

Total protein extracts were obtained from the cerebral cortex of 1-day postnatal SVCT2tg, SVCT2$^{+/-}$, and SVCT2^{wt} mice as previously described (Salazar et al., 2014). Primary antibodies used were anti-NeuN (1:1000, EMD Millipore, USA), anti-GFAP (1:2000, #Z0334, DAKO, Carpinteria, CA, USA), anti-βIII- tubulin (Tuj1; 1:1500; Promega, Madison, Wisconsin, USA) anti-GAPDH (1:5000, MAB374, EMD Millipore, USA), anti-phospho p44/42 MAPK (ERK1/2, Thr202/Tyr204) (1:2000, Cell Signaling Technology, USA), anti-p44/42 MAPK (ERK1/2) (1:3000, Cell Signaling Technology, USA), anti-phospho-AKT (Ser473) (1:2000, Cell Signaling Technology, USA), anti-phospho-AKT (Thr308) (1:2000, Cell Signaling Technology, USA), anti-AKT (1:3000, Cell Signaling Technology, USA), anti-phospho-GSK3β (1:2000, Cell Signaling Technology, USA), anti-GSK3β (1:3000, Cell Signaling Technology, USA), anti-phospho mTOR (1:2000, Cell Signaling Technology, USA), anti-mTOR (1:2000, Cell Signaling Technology, USA), and anti-phospho-PDK1 (1:1000, Cell Signaling Technology, USA), diluted in blocking solution overnight at 4°C. Following incubation with respective IRDye® secondary antibodies (1:10,000, LI-COR) for 1 h at room temperature and visualization of signal on Licor Odyssey CLx system.

2.14 | Surface analysis and morphological parameters of primary cultures

Images acquired by confocal microscopy were subsequently analyzed by ImageJ software (National Institutes of Health). The average cell surface area was determined in each condition by manually tracing a region of interest (freehand selection tool), which covered the outline of each cell present in the field. On the other hand, the percentage of cells exhibiting processes was quantified, as well as the average length of these processes, which were defined as an extension that was longer of the diameter of the cell body. The cellular process length was determined by manually delineating the cellular process of interest, using the freehand line tool. Regarding the percentage of cells with astrocyte or radial glia phenotype, the abundance of the phenotype was determined through the multi-point tool with respect to the total number of cells in each field for each condition.

2.15 | Statistical analysis

To study SVCT2 mRNA expression through qRT-PCR, the data were analyzed by Student's *t*-test, comparing the different stages studied with respect to 1-day postnatal. On the other hand, the comparison between the SVCT2^{wt}, SVCT2^{tg}, SVCT2$^{+/-}$ mice groups, the percentage of cells with processes; average length of these; number of processes per cell, was performed by Student's *t*-test and one- or two-way ANOVA followed by Tukey's post hoc test. In western blot assays, the comparison of the band intensity between each normalized group was performed using one-way ANOVA following the Tukey's post hoc multiple comparisons test. In all cases described above, significance was assigned for a p value <0.05.

3 | RESULTS

3.1 | IRG cells are found in a postnatal context

For IRG cells detection, immunohistochemical assays with anti-vimentin were performed on 1-day-old rat brain tissues and were distinguished using two-photon microscopy which allowed us to have an increased imaging depth, obtaining highly localized photochemistry in thick samples (Figure 1a). It was noticed that there was a greater population of thin elongated radial processes in the dorsal area of the lateral ventricle compared to the lateral and ventral zone of the lateral ventricles. These processes begin with close contact on the VZ projecting radially toward the cortex until reaching, through an end foot, the pial surface (Figure 1a, yellow arrows). The abundance and morphology of IRG cells were also analyzed by confocal microscopy, with classical structural markers GFAP and vimentin, as well as the enzymatic marker 3-PGDH (Figure 1b). GFAP not only allows us to visualize IRG processes but also to observe astrocytes (Figure 1b, continuous arrows), as both cell types are positive for this marker. Analysis of GFAP immunogold showed gold particles localized to the bundles of intermediate filaments of IRG cells (Figure 1c, arrows in black) and in astrocyte projections having contact with blood vessels (Figure 1c, dashed lines and red arrows). Also, multiple gold particles were observed in the neuropil of the cortex, which is where the astrocytic processes are located. For an in vivo identification of IRG cells, intraventricular injections of an eGFP-expressing Adenovirus (Ad-GFP) were performed in the P1 rat brain (Figure 1d). Likewise, intraventricular injections of an eGFP-plasmid followed by electroporation allowed the detection of IRG cells (Figure 1e). In both cases, it was clearly observed that transduced and electroporated eGFP-positive cells in the VZ-SVZ had the distinctive morphology of RG cells, with the cell body located between de V-SVZ and thin radial processes extending toward the pial surface (Figure 1d,e).

3.2 | The ascorbic acid transporter, SVCT2, is ventricularly polarized in IRG cells

Laser microdissection of the VZ and SVZ in the dorsal areas of the lateral ventricles followed by qRT-PCR was used to analyze SVCT2 expression (Figure 2a). There was no significant difference in SVCT2 expression between the first and fourth postnatal day and this expression decreased to be significantly lower on day 8. However, from postnatal day 12, SVCT2 expression increased significantly (Figure 2b). As a positive control, SVCT2 mRNA analysis of the total cerebral cortex was performed, and as expected, SVCT2 expression increased significantly as development proceeds (Figure 2c). This increase was consistent with the fact that cortical neurons express the AA transporter and as corticogenesis proceeds, the number of neurons that express SVCT2

10981136, 0, Downloaded from https://onlinelibrary.wiley.com/doi/10.1002/glia.24498 by Chun-Consorcio De Bibliotecas, Wiley Online Library on [26/01/2024]. See the Terms and Conditions (https://onlinelibrary.wiley.com/terms-and-conditions) on Wiley Online Library for rules of use; OA articles are governed by the applicable Creative Commons License

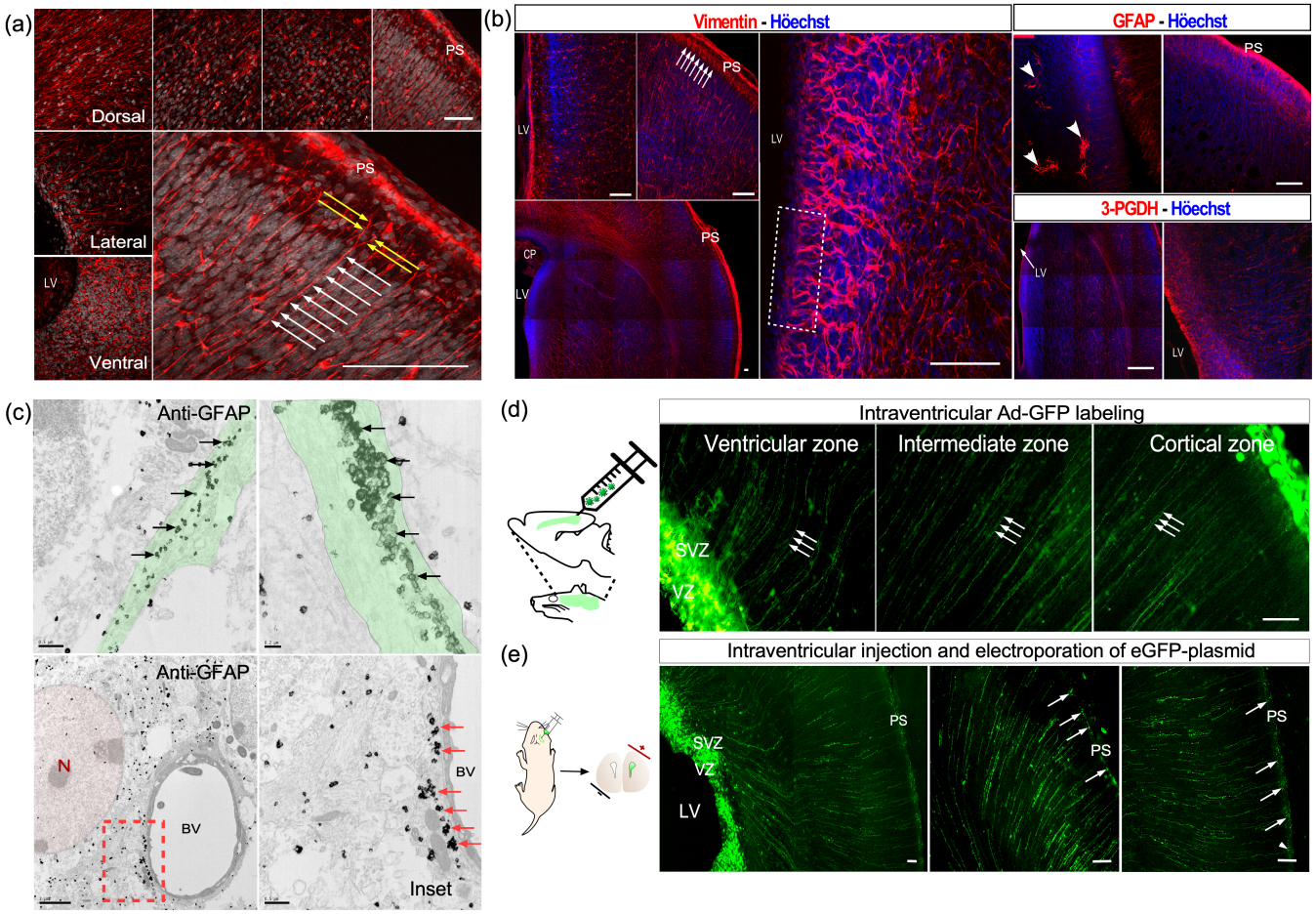

FIGURE 1 Analysis of the distribution of IRG cells in postnatal rat brain. (a) Two-photon microscopy analysis of 1-day postnatal rat brains in different regions of the lateral ventricle. IRG processes were identified with vimentin (red) and nuclei with Höechst (gray). White arrows indicate a radial process; yellow arrows show an end foot of a IRG cell. (b) Confocal microscopy analysis for vimentin, GFAP and 3-PGDH (red) in frontal sections of 1-day-old rat brain in the V-SVZ and cerebral cortex. Dashed arrows indicate IRG cells endfoot. Inset shows the IRG cells processes in contact with the V-SVZ and solid arrows indicate the presence of astrocytes in GFAP staining. Nuclei were visualized with Höechst (blue). (c) Ultrastructural analysis and GFAP immunogold in 3-day postnatal rat brains. Gold particles are indicated by black arrows in IRG processes (green colored) and in cellular projections that have contact with blood vessels (red dotted box and red arrows). Multiple gold particles were distinguished in the neuropil of the cerebral cortex. (d) Images acquired by confocal microscopy of 3-day-old rat brains transduced with adenovirus-siβGal-eGFP injected ventrally at postnatal day 1. Arrows indicate a radial process. (e) Analysis of frontal slices from 3-day postnatal rats electroporated intraventricularly with the eGFP plasmid at postnatal day 1. Arrows indicate the end foot of a IRG cells in contact with the pial surface. PS, pial surface; LV, lateral ventricle; VZ, ventricular zone; SVZ, subventricular zone; BV, blood vessel; N, neuroblasts. Scale bar: 100 μm (a, b); 50 μm (d, e).

also increases (Caprile et al., 2009; Garcia Mde et al., 2005; Mun et al., 2006; Nualart et al., 2012; Oyarce et al., 2018; Salazar et al., 2014; Salazar et al., 2017; Tsukaguchi et al., 1999).

To further define the distribution of SVCT2 mRNA, in situ hybridization experiments for SVCT2 were performed in rat brains of 1, 4, and 8 days (Figure 2d–f). At P1, there was a high hybridization signal for SVCT2 in the dorsal, lateral, and ventral VZ and SVZ of the lateral ventricles (Figure 2d) while at P4, this signal was only distinguished in the dorsal region of the ventricle (Figure 2e). In 8-day-old brains, there was high reactivity for the SVCT2 probe in the ventral area of the ventricle (Figure 2f) and like what was observed at P4, the lateral region remained with a scarce signal of hybridization which increases as it approaches the dorsal region of the ventricle (Figure 2f).

Additionally, SVCT2 presence in the VZ and SVZ was determined by immunohistochemical assays in the cerebral cortex of 1-day postnatal rat (Figure 2g). For this analysis, antibodies against 3-PGDH and vimentin were used for the detection of IRG cells, as well as an affinity-purified polyclonal antibody that recognizes an extracellular domain of rat and human SVCT2. Our analyses showed immunoreactivity of SVCT2 in the VZ and SVZ of the dorsal region of the lateral ventricles (Figure 2g), co-localizing at the apical level with the RG markers (arrows in Figure 2g).

To perform more detailed studies of the ventricular polarization of SVCT2, ultrastructural analyses were carried out by transmission electron microscopy. Thus, 3-day-old rat brains showed in the ventricular zone cellular processes of IRG cells with an electron-lucid

10981136, 0, Downloaded from https://onlinelibrary.wiley.com/doi/10.1002/glia.24498 by Cbua-Consorcio De Bibliotecas, Wiley Online Library on [26/01/2024]. See the Terms and Conditions (https://onlinelibrary.wiley.com/terms-and-conditions) on Wiley Online Library for rules of use; OA articles are governed by the applicable Creative Commons License

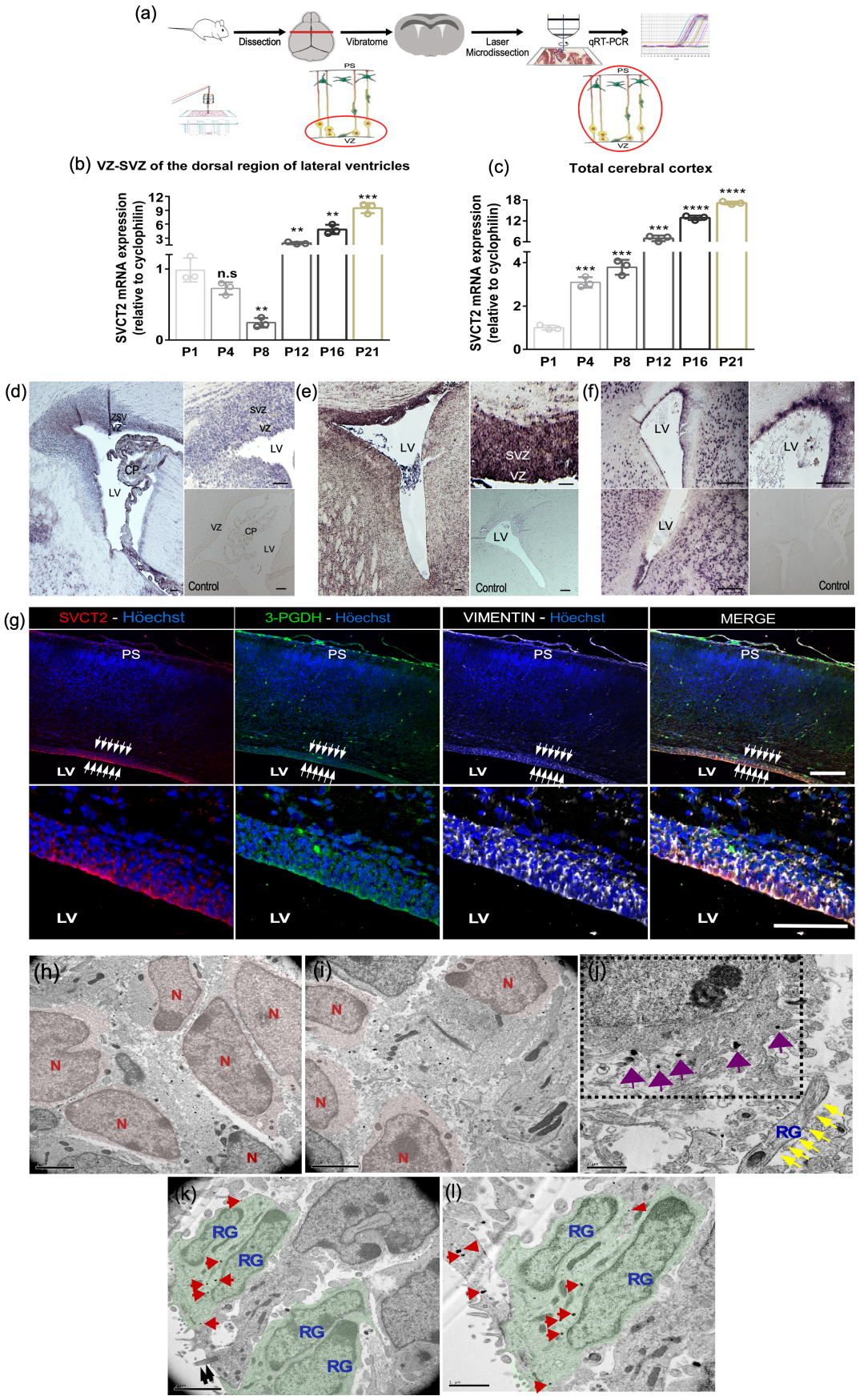

FIGURE 2 Legend on next page.

10981136, 0, Downloaded from https://onlinelibrary.wiley.com/doi/10.1002/glia.24498 by Chua-Consorcio De Bibliotecas, Wiley Online Library on [26/01/2024]. See the Terms and Conditions (https://onlinelibrary.wiley.com/terms-and-conditions) on Wiley Online Library for rules of use; OA articles are governed by the applicable Creative Commons License

cytoplasm (Figure 2h–l, highlighted in green-RG), as well as cell expansions corresponding to primary cilia, which are in contact with the CSF (Figure 2k, black arrows). The intermediate zone of the cortex was populated with numerous neuroblasts (Figure 2h,i, highlighted in red-N) which are characterized by having a heterochromatic nucleus and an electron-dense cytoplasm. More mature neurons were distinguished in the outer cortical region (Figure 2j, inset). Immunogold ultrastructural staining of SVCT2 showed the transporter located in the ventricular zone of the lRG cells (Figure 2k,l, red arrows), but not in the basal processes of this cell (Figure 2j, yellow arrows). Also, it should be noted that some neuroblasts and mature neurons were immunoreactive for SVCT2. Collectively, these results indicate that SVCT2 is ventricularly polarized in lRG cells.

3.3 | Characterization of lRG cells throughout postnatal development

For further characterization of lRG cells, immunohistochemical studies were performed on rat brains collected at 1, 4, 12, and 16 postnatal days using: anti-vimentin for lRG cells visualization, glucose transporter 1 (GLUT1) to analyze ependymal cells and blood vessels, and SVCT2 antibody (Figures 3a,b and S1). At postnatal day 1, as was foreseeable, immunoreactivity for vimentin was identified in the lRG cell processes and in the macrocirculation blood vessel system in the outer cortical region (Figure 3a, arrows). Regarding detection with anti-GLUT1, it was dimly distinguished in the ventrolateral region of the ventricles (Figure 3a, inset). Also, it was visualized in the microcirculation, mainly in the regions proximal to the lateral ventricle as well as in the microcirculation (arrows in Figure 3a). SVCT2 was preferentially detected in the vessels of the macrocirculation (Figure 3a, arrows), in VZ-SVZ, throughout the cerebral cortex (Figure 2a), and in the choroid plexuses (Figure 3a), as has been previously described (Ulloa et al., 2019).

In 4-day-old brains, a generalized decrease in the number of lRG cells immunoreactive for vimentin was observed in the lateral ventricles, which is more evident in the ventrolateral region (Figure 3b). However, lRG cells immunoreactive for vimentin and SVCT2 are still maintained in the dorsal ventricular region (Figure 3b), where the lRG cell processes were identified to extend radially from the ventricular region toward the external cortical cortex (Figure 3b). Regarding the macrocirculation observed in the external cortical region, these continue to be immunoreactive for GLUT1, but not for SVCT2 (Figure 3b). In addition, a higher number of GLUT1, SVCT2 and vimentin-positive ependymal cells present in the ventrolateral regions of the ventricle were detected (Figure 3b, lower part of the panel).

As development proceeds, in the 12- and 16-day postnatal brains, a sharp decrease in the number of lRG cell processes was observed and those remaining do not exhibit a radial morphology, on the contrary; they were distinguishable in a branched form (Figure S1a,b) and even some vimentin-positive processes were visualized with immature astrocytic morphology in the ventral region of the ventricle (Figure S1a, arrows). In addition, no vimentin-positive processes were distinguished reaching the pial surface or in the external cortical region (Figure S1a,b). In parallel, ependymal cells are observed populating large areas of the ventrolateral ventricular region, being immunoreactive for vimentin, GLUT1, and SVCT2 (Figure S1a,b, inset). At 16 days postnatal, GLUT1 was also observed in the dorsal region of the ventricle (Figure S1b, dashed inset), indicating a more terminal maturation phase of the ependyma.

As lRG cells decrease in the ventricular wall, the presence of ependymal cells increases, which present GLUT1. Therefore, the expression of GLUT1 was analyzed by laser microdissection of the VZ and the SVZ of the dorsal ventricular region and subsequent qRT-PCR. Interestingly, in the dorsal ventricular wall, from 8 postnatal days onwards, GLUT1 mRNA increases steadily and significantly during postnatal stages (Figure 3c).

Together, this data showed that SVCT2 is present between the first and fourth postnatal day in the dorsal area of lateral ventricles, the same period in which a high number of lRG cells are present. Then, through the course of development, lRG cells disappear from the lateral ventricles and it is the ependymal cells that begin to populate the ventricle in a ventrodorsal manner expressing SVCT2 and GLUT1.

Additionally, immunohistochemical analyzes along with confocal microscopy were performed on rats at 1 and 4 postnatal days with Sox2 antibody, a transcription factor whose function is essential in the maintenance of stem cell self-renewal and pluripotency (Zhang &

FIGURE 2 Analysis of SVCT2 distribution in the cerebral cortex of postnatal rats. (a) Scheme of the experimental approach used to isolate and analyze the SVCT2 expression in the dorsal V-SVZ and total cerebral cortex. (a, b) The microdissected areas that were analyzed by qRT-PCR are indicated. Quantification of SVCT2 mRNA expression using laser microdissection and qRT-PCR at 1-, 4-, 8-, 12-, 16- and 21-day postnatal stages in the dorsal V-SVZ of the lateral ventricles (b) and total cerebral cortex (c). Statistical *t*-student analysis was used to compare stage 1 day versus P4, P8, P12, P16 and P21 (*$p < 0.05$; **$p < 0.01$; ***$p < 0.001$; ****$p < 0.0001$); n.s. = not significant. (d and f) Frontal sections of 1 (d), 4 (e) and 8-day (f) postnatal rat brain were hybridized using a digoxigenin-labeled antisense-specific riboprobe against SVCT2 mRNA. (g) Immunohistochemical analysis by confocal microscopy of SVCT2 (red) and radial glia cells, 3-PGDH (green) and vimentin (white) in 7 μm slices of rat cerebral cortex 1 day postnatal. Nuclei were visualized with Höechst (blue). Arrows indicate immunoreactivity of SVCT2 and RG cells markers in V-SVZ of the lateral ventricles. (h–l) Ultrastructural analysis and SVCT2 immunogold in 3-day postnatal rat brains. (h, i) Multiple neuroblasts (N, pink colored) were found in the intermediate zone of the cortex. (j) Gold particles are indicated with purple arrows in more differentiated neurons located in the outer cerebral cortex (inset), yellow arrows show a lRG cell process in the outer cortex. (k, l) Gold particles in lRG processes (RG, green colored) are indicated with red arrows. Black arrow indicates a primary cilium (k). LV, lateral ventricle; VZ, ventricular zone; SVZ, subventricular zone; CP, choroid plexus: PS, pial surface. Scale Bar: 50 μm (d–f); 100 μm (g).

10981136, 0, Downloaded from https://onlinelibrary.wiley.com/doi/10.1002/glia.24498 by Chun-Consorcio De Bibliotecas, Wiley Online Library on [26/01/2024]. See the Terms and Conditions (https://onlinelibrary.wiley.com/terms-and-conditions) on Wiley Online Library for rules of use; OA articles are governed by the applicable Creative Commons License

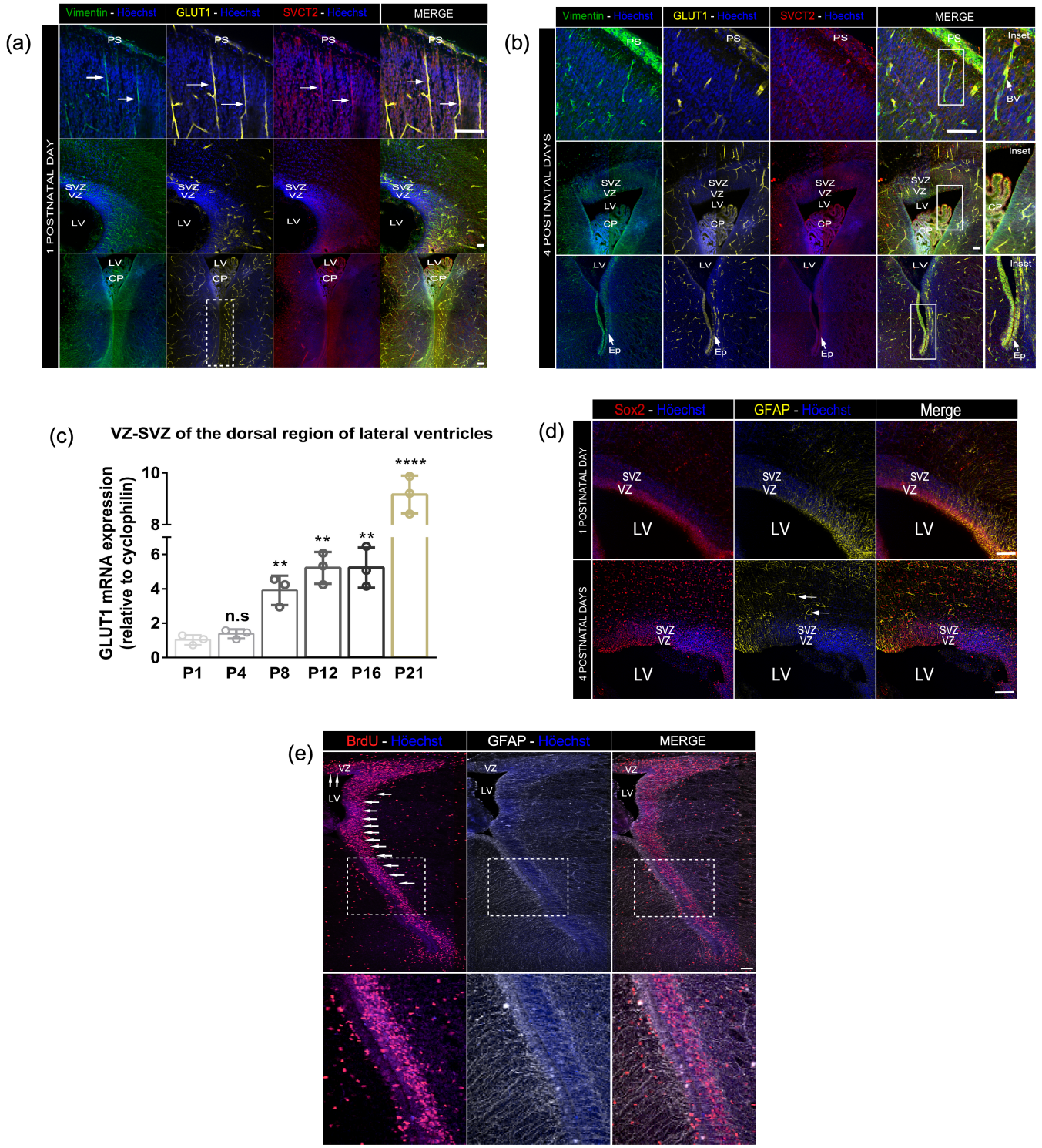

FIGURE 3 Characterization of lRG cells in the postnatal cerebral cortex. (a) Confocal microscopy images of the cerebral cortex of 1-day postnatal rat brains for vimentin (green), GLUT1 (yellow) and SVCT2 (red). Inset shows GLUT1 reactivity in the ventral zone of the lateral ventricle. Höechst (blue) shows the nuclei. (b) Images of the cerebral cortex of 4-day postnatal brains. Cells located in the ventral zone of the lateral ventricle immunoreactive for GLUT1, vimentin and SVCT2 are indicated (inset). Cell nuclei were visualized with Höechst (blue). (c) Quantitative analysis of GLUT1 mRNA expression in the dorsal V-SVZ of the cerebral cortex. t-student statistical analysis was used to compare stage 1 day versus P4, P8, P12, P16 and P21 (*$p < 0.05$; **$p < 0.01$; ***$p < 0.001$; ****$p < 0.0001$); n.s. = not significant. P: Postnatal. (d) Immunohistochemical analysis by confocal microscopy for Sox2 (red) and GFAP (yellow). Arrows indicate cells with astrocytic morphology. Höechst (blue) shows the nuclei. (e) BrdU-positive cells (red) in the V-SVZ (arrows) and immunoreactivity for GFAP (white) along the ventricle. Inset shows the digitally enhance area of the V-SVZ. Höechst (blue) shows the nuclei. LV, lateral ventricle; PS, pial surface; CP, choroid plexus; VZ, ventricular zone; SVZ, subventricular zone. Scale bar: 100 µm (a, b, d); 200 µm (e).

10981136, 0, Downloaded from https://onlinelibrary.wiley.com/doi/10.1002/glia.24498 by Cbua-Consorcio De Bibliotecas, Wiley Online Library on [26/01/2024]. See the Terms and Conditions (https://onlinelibrary.wiley.com/terms-and-conditions) on Wiley Online Library for rules of use; OA articles are governed by the applicable Creative Commons License

Cui, 2014). In addition, anti-GFAP was used to observe RG cells and astrocytes (Figure 3d). In 1-day-old rat brains, results showed immunoreactivity for Sox2 in the VZ and SVZ of the lateral ventricle, which decreases and expands throughout the cortex in 4 postnatal days (Figure 3d). As for GFAP-positive cells displaying astrocytic morphology were clearly distinguishable at postnatal day 4 (arrows in Figure 3d), indicating that IRG cells that postnatally populate the ventricular wall were positive for a well-known marker for stem cells. Another stem cell characteristic is its unique ability to self-renew. To determine whether IRG cells remain proliferative, a single bromodeoxyuridine (BrdU) intraventricular injection was performed in 1-day rats (Figure 3e) and the animals were sacrificed 2 days post-injection. The results showed that there was a population of BrdU-positive cells located mainly in the V-SVZ of the lateral ventricles (Figure 3e, arrows). In addition, positive BrdU cells located in the cerebral cortex were observed, which probably correspond to daughter cells from IRG cells (Figure 3e).

3.4 | IRG cells maintain neurogenic differentiation in postnatal stages

To analyze in situ IRG cell differentiation, intraventricular injections using adenoviral particles expressing the eGFP reporter gene were performed in 1-day-old rats. After 5 days, the animals were sacrificed and transduced brain sections were analyzed by confocal microscopy (Figure 4a). The results showed a high density of eGFP-positive labeled cells in the ventricular region (Figure S2a). Radial processes were observed to start from the VZ and SVZ of the ventricle (Figure 4a, yellow arrows), extending radially toward the pial surface (Figure 4a, white arrows). In addition, cells with a migratory neuronal morphology were observed (Figure 4a, continuous red arrows). Some of these eGFP-positive cells migrate using the basal processes of the RG cells as a guide (Figure 4a, dashed red arrows and Figure S2c, white and yellow arrows). eGFP-positive cells were distinguished by possessing an elongated cell body that narrows in the direction of migration, a structure known as the leading process (Figure 4a, blue arrowhead). These cells with migratory neuronal phenotype were detected in the intermediate zone, as well as in the uppermost layers of the cerebral cortex (Figure 4a), and none of them were found in the rostral migration stream (RMS). Thus, the results showed that adenovirus is selectively transduced in the IRG cells, as well as in cells originating from them, which exhibit a migratory neuronal phenotype.

Complementarily, earlier and later stages of post-adenoviral injection were analyzed (Figure S2b). In these experiments, rats were injected intraventricularly at the 1-day postnatal stage and analyzed at 2- and 12-day post-transduction. In line with what was previously observed, at 2 days post-injection, cells with migratory neuronal phenotype were detected in the cerebral cortex, mainly in a clustered manner (Figure S2b). These clusters of migratory cells were essentially visualized in the vicinity of the ventricle and in the intermediate zone, but not in the outer cortical region (Figure S2b). At later stages, after

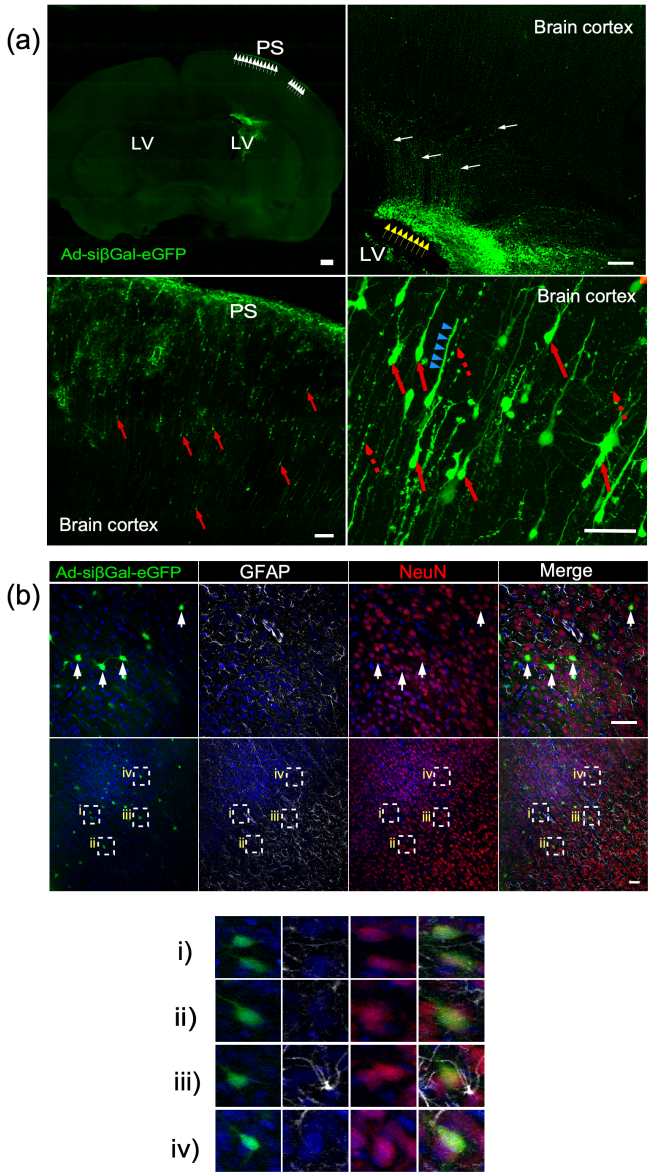

FIGURE 4 Adenoviral transduction in the ventricular and subventricular region of the lateral ventricles. (a) Confocal microscopy of the transduction performed with eGFP adenovirus at 1-day and analyze at 6-day postnatal. Radial processes and cells with migratory neurons morphology were observed. White arrows indicate positive eGFP signal in the pial surface region. Yellow arrows show adenoviral transduction in the V-SVZ. Light blue arrows indicate a cell leading process of a migrating neuron and radial processes are indicated (red arrows) in the 3D reconstruction obtained by stacking on the Z-axis (Z-stack). (b) Representative immunohistochemical images for GFAP (white) and NeuN (red) of 17-day-old rat brains injected ventricularly with adenovirus-eGFP at postnatal day 1. Some eGFP-positive cells are indicated (arrows) co-localizing with the neuronal marker NeuN. (i–iv) Digital magnification of i-iv inset, respectively. Nuclei were visualized with Höechst (blue) in all images. LV, lateral ventricle; PS, pial surface. Scale bar: 100 μm (A, tile scan 1 mm); 50 μm (B).

12 days post-adenoviral transduction, eGFP-cells with a neuronal phenotype in the maturation process were identified, as growth and arborization of dendrites were observed (Figure S4b).

10981136, 0, Downloaded from https://onlinelibrary.wiley.com/doi/10.1002/glia.24498 by Cbua-Consorcio De Bibliotecas, Wiley Online Library on [26/01/2024]. See the Terms and Conditions (https://onlinelibrary.wiley.com/terms-and-conditions) on Wiley Online Library for rules of use; OA articles are governed by the applicable Creative Commons License

To accurately determine the neuronal identity of cells with a migratory neuronal phenotype, immunohistochemistry with anti-NeuN (neuronal nuclei), βIII-tubulin, and anti-GFAP was performed. The results confirmed that eGFP-positive cells with neuronal morphology correspond to neurons, co-localizing with NeuN (Figure 4B) and with βIII-tubulin (Figure S2c, inset). In addition, these cells did not exhibit positive labeling for the glial marker GFAP, ruling out that they correspond to astrocytes (Figure 4b). On the other hand, eGFP-positive cells located in VZ-SVZ colocalized with the Sox2 marker (Figure S2d, continuous inset). In summary, these results showed that eGFP-positive cells were positively labeled for neuronal markers (NeuN-βIII-tubulin) and for RG markers (vimentin-Sox2) and not for astrocytic markers (GFAP), suggesting that some IRG cells continue to generate neuronal cells in a postnatal context directed to more superficial layers of the cerebral cortex.

3.5 | Role of AA and its transporter, SVCT2, in IRG-like cells differentiation in vitro

Once the presence of IRG cells was established in a postnatal context, we proceeded to evaluate the AA effect on an enriched primary culture of IRG-like cells. For this purpose, a primary culture enriched in IRG-like cells was generated (Figure S3a). After 4 days in vitro, IRG-like cells were distinguished positive for Sox2, nestin, and SVCT2 and virtually negative for GFAP antibody (Figure S3a, yellow arrows). In addition, IRG-like cells were observed morphologically with two fine elongated processes, which contrasted with the astrocytes; cells that presented a polygonal to fusiform and flat morphology without cellular processes (Figure S3a, white arrows). Quantification of cell phenotype in this primary culture showed that more than 70% of the cells corresponded to IRG-like cells and concordantly, a similar percentage of cells with processes was determined. When enriched IRG-like cell primary culture was maintained for 10 days in vitro, it was found to be composed almost entirely of astrocyte-like morphology cells, which were GFAP positive while negative for Sox2 and nestin (Figure S3b). Interestingly, IRG-like cell primary cultures supplemented with physiological concentrations of AA (200 μM) showed abundant cells with radial morphology (41.21 ± 7.95%), a percentage that was significantly higher when compared to the control (4.48 ± 0.99%) (Figure 5a,b). Also, 42.14 ± 8.49% of cells showed cellular processes in primary cultures supplemented with AA and only 3.57 ± 1.80% of cells displayed cellular processes in the control (Figure 5c). Interestingly, the length of the processes in AA-treated cultures was approximately 1.7-fold longer than that observed in the control (Figure 5d). Finally, as IRG cells have a smaller cell area than astrocytes, by averaging the cell surface area, it was established that the cells present an area of 456.6 ± 33.7 μm^2 in the primary culture treated with AA, which is significantly smaller than the primary culture that was not treated with AA (2702.6 ± 53.2 μm^2) (Figure 5e).

Next, we evaluate the effect of different levels of SVCT2 on IRG differentiation. Based on previous findings showing that $SVCT2^{+/-}$ and $SVCT2^{tg}$ mice exhibit significantly decreased and increased AA levels, respectively (Harrison et al., 2012; Sotiriou et al., 2002), we performed enriched IRG-like cell primary cultures from these transgenic mice (Figure 5f–k). After 4 and 7 days in vitro, cells were fixed and analyzed by immunohistochemistry with anti-vimentin to visualize cell morphology. To determine if significant differences exist, each condition was compared with SVCT2-*wild type* primary culture. After 4 days in vitro, primary cultures from $SVCT2^{wt}$ mice showed both, cells with radial- (54.98 ± 7.44%) and astrocytes-like morphology (45.01 ± 7.44%) (Figure 5f,g). Interestingly, in primary cultures obtained from $SVCT2^{+/-}$ brains, the percentage of astrocytes increased considerably (98.08 ± 1.39%) and the percentage of IRG-like cells (1.93 ± 1.39%) was significantly decreased (Figure 5f). On the contrary, when analyzing the composition of the primary culture obtained from $SVCT2^{tg}$ brains, the cells mostly present corresponded to IRG-like cells (84.67 ± 3.73%) and to a lesser extent to astrocytes (15.33 ± 3.73%) (Figure 5g). Quantitative analysis of the percentage of cells exhibiting processes showed that in the $SVCT2^{wt}$ primary culture, 50.52 ± 6.15% of cells showed processes, whereas in $SVCT2^{+/-}$ cultures it decreased significantly exhibiting only 1.93 ± 1.39% of cell with processes (Figure 5h). In contrast, in $SVCT2^{tg}$ cultures, cells with processes increased significantly to 81.13 ± 3.17% (Figure 5h). Surprisingly, the length of processes in cells from $SVCT2^{tg}$ mice increased 2.1-fold relative to cells isolated from $SVCT2^{wt}$ animals (Figure 5i). Furthermore, the area presented by the cells composing the primary $SVCT2^{+/-}$ culture was determined to be 457.6 ± 28.7 μm^2, being significantly larger for the control culture (194.3 ± 10.1 μm^2), while the cell area present in the $SVCT2^{tg}$ culture was 310.0 ± 21.3 μm^2 (Figure 5j). After 7 days in vitro, cell cultures from $SVCT2^{wt}$ and $SVCT2^{+/-}$ brains had 100% cells with astrocytic phenotype (Figure 5k,l), and no cells with processes (Figure 5m). On the other hand, cells comprising the primary culture enriched in IRG cells from $SVCT2^{tg}$ mouse brains showed that 79.35 ± 5.63% of cells exhibited a IRG cell phenotype (Figure 5l), which was consistent with the percentage of cells exhibiting processes; 77.97 ± 6.27% (Figure 5m) and these processes exhibit 1.6 times longer length than those observed at 4 days in vitro. Finally, the average cell surface area of this primary culture was significantly smaller than the cell surface area of the cells composing the primary culture from $SVCT2^{wt}$ mouse brains. This data suggests that the cells composing the primary $SVCT2^{tg}$ culture correspond mainly to IRG-like cells and astrocytes in the early stages of maturation and cells in the primary culture from $SVCT2^{+/-}$ mice were composed mostly of astrocytes.

3.6 | Overexpression of SVCT2 in IRG cells in vivo, leads to the generation of migratory cells with rounded morphology and positive for migratory neuron marker

To generate SVCT2 overexpression and thereby increase AA incorporation into IRG cells, a plasmid encoding for SVCT2-eGFP was injected intraventricularly into 1-day-old rats and subsequently electroporated. Interestingly, at all post-electroporation

10981136, 0, Downloaded from https://onlinelibrary.wiley.com/doi/10.1002/glia.24498 by Cbua-Consorcio De Bibliotecas, Wiley Online Library on [26/01/2024]. See the Terms and Conditions (https://onlinelibrary.wiley.com/terms-and-conditions) on Wiley Online Library for rules of use; OA articles are governed by the applicable Creative Commons License

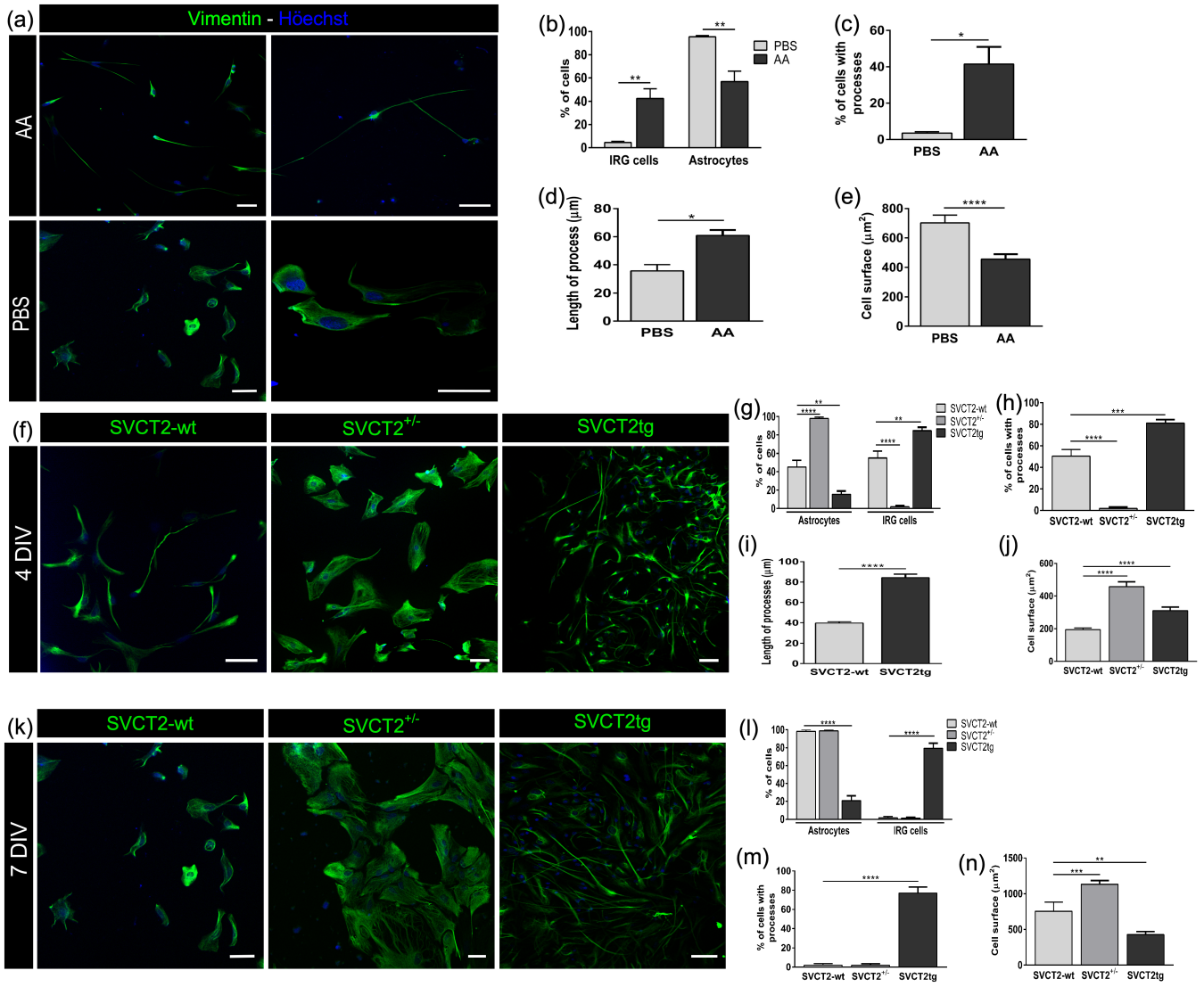

FIGURE 5 Analysis of AA and SVCT2 levels effects in primary cultures enriched in IRG cells. (a) Representative confocal images of primary culture enriched in IRG cells treated for 7 days with AA or PBS (control) every 24 h. (b–e) Quantitative analysis of cells percentage with radial and astrocytic phenotype, percentage of cells exhibiting processes, average cell surface area and length of processes are indicated. (f–n) Immunocytochemistry and quantitative analysis of 4 days (g–j) and 7 days (l–n) in vitro primary cultures enriched in IRG cells obtained from 1-day postnatal cerebral cortex of SVCT2^{wt}, SVCT2$^{+/-}$ and SVCT2^{tg}. In all images, cell processes were observed with vimentin (green) and nuclei with Höechst (blue). For statistical analyses, (b–e, i) Student's *t*-test; (h, j, m, n) one-way ANOVA or (g, l) two-way ANOVA were performed. F values for (g, h, j, l–n): 120.1, 78.5, 46.7, 395.1, 128.0, 34.8, respectively. ANOVA analyses were followed by Tukey's post hoc test to determine differences between SVCT2^{wt} with SVCT2$^{+/-}$ or SVCT2^{tg}. (*$p < 0.05$; **$p < 0.01$; ***$p < 0.001$; ****$p < 0.0001$). $n = 3$. Scale bar: 50 µm.

stages analyzed, it was observed that SVCT2-eGFP-positive cells did not present RG morphology, but instead a rounded cell morphology (Figure 6a). After 1-day post-electroporation, SVCT2-eGFP cells were mainly located in the V-SVZ of the lateral ventricle (Figure 6a). However, after 2 days post-electroporation, most SVCT2-eGFP cells were visualized in the intermediate zone and few cells in the V-SVZ (Figure 6a). Furthermore, when observed 3 days post-electroporation, SVCT2-eGFP cells were distinguished in a shallower region of the intermediate zone (Figure 6a). At later stages, after 7 days post-electroporation, SVCT2-eGFP cells were observed in the outer cerebral cortex and no SVCT2-eGFP-positive cells were visualized in the V-SVZ, nor in the intermediate zone of the cerebral cortex (Figure 6a). Thus, it was observed that the electroporated cells migrated from the ventricular and subventricular zone, toward different layers of the cerebral cortex.

On the other hand, as expected, cells incorporating the control-eGFP plasmid displayed the RG phenotype. This morphology was observed in eGFP-positive cells at all post-electroporation stages analyzed; cell bodies located mainly in the lateral ventricles and radial processes extended toward the pial surface were visualized (Figure 6a). This observation allowed us to confirm that IRG both can be reliably detected in rat postnatal brains either by adenoviral labeling or by electroporation mediated-gene transfer.

10981136, 0, Downloaded from https://onlinelibrary.wiley.com/doi/10.1002/glia.24498 by Cbua-Consorcio De Bibliotecas, Wiley Online Library on [26/01/2024]. See the Terms and Conditions (https://onlinelibrary.wiley.com/terms-and-conditions) on Wiley Online Library for rules of use; OA articles are governed by the applicable Creative Commons License

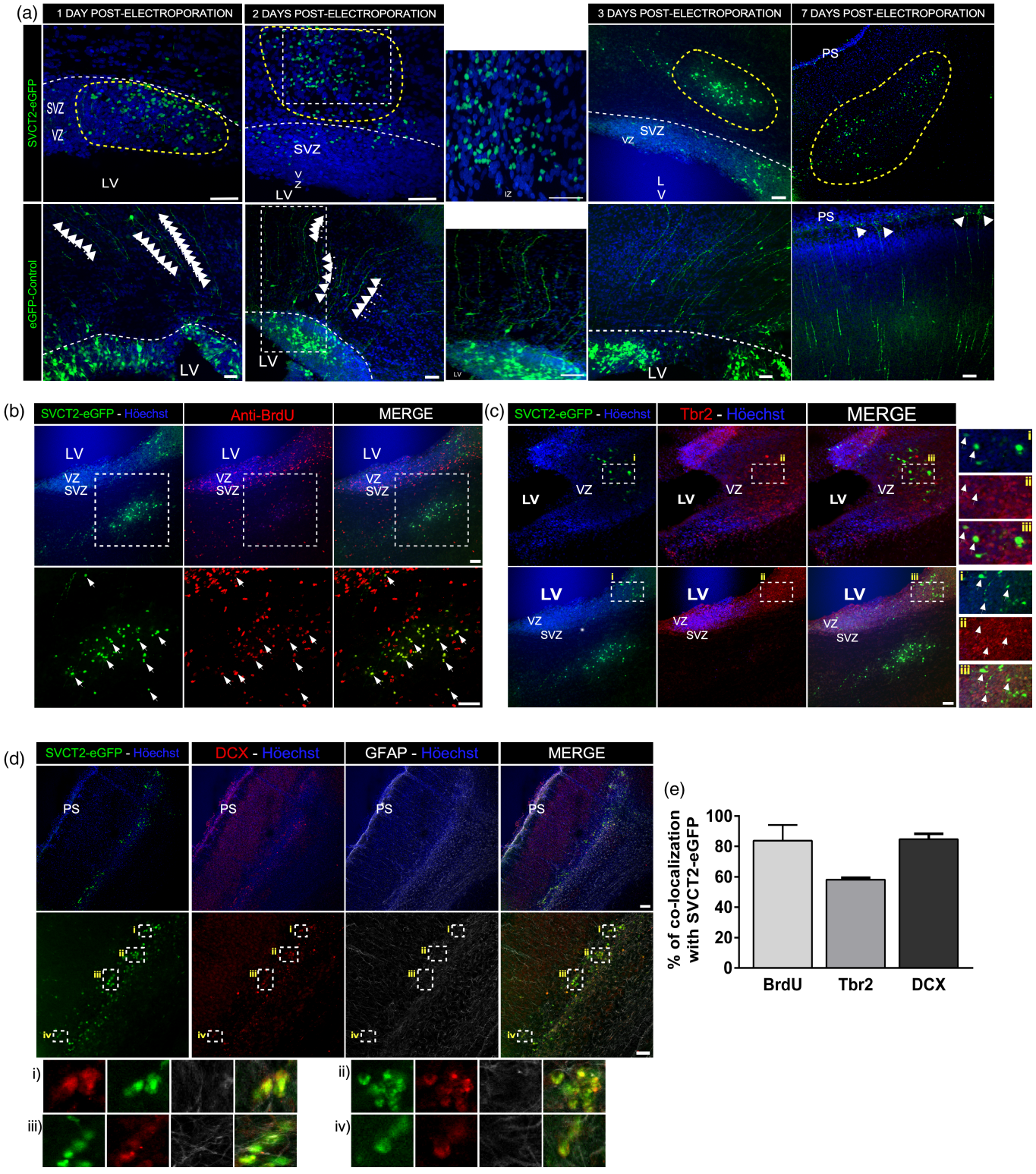

FIGURE 6 Legend on next page.

Because of the morphology analyzed and the high co-localization with anti-3-PGDH (90.47 ± 2.02%, Figure 4b), it was established that control-eGFP positive cells correspond to IRG cells, while SVCT2-eGFP cells do not share the morphology of the RG, nor the co-localization with the 3-PGDH antibody (Figure S4b). The evident morphological change presented by SVCT2-overexpressing cells, compared to the control, prompted us to analyze the identity of SVCT2-eGFP-positive cells by immunohistochemistry. First, as confirmation and as expected, a high co-localization (97.03 ± 1.94%) between SVCT2-eGFP-positive cells with the anti-SVCT2 antibody

10981136, 0, Downloaded from https://onlinelibrary.wiley.com/doi/10.1002/glia.24498 by Cbua-Consorcio De Bibliotecas, Wiley Online Library on [26/01/2024]. See the Terms and Conditions (https://onlinelibrary.wiley.com/terms-and-conditions) on Wiley Online Library for rules of use; OA articles are governed by the applicable Creative Commons License

was observed (Figure S4a). Furthermore, intraventricular injection of BrdU together with SVCT2-eGFP plasmid followed by electroporation was performed. A co-localization of 81.76 ± 10.43% was observed between SVCT2-eGFP-positive cells and BrdU (Figure 6b,e). Accordingly, it was determined that most SVCT2-eGFP cells were derived from proliferative cells—IRG—and/or are proliferating cells.

IPs are characterized by having a spherical morphology, being highly proliferative cells, being located mainly in the SVZ, and generating only neurons (Hevner, 2019). To determine whether SVCT2-eGFP cells correspond to IPs, immunohistochemistry was performed with the Tbr2 antibody, a transcription factor found exclusively in these cells, and the VZ, SVZ, and the inner region of the intermediate zone were analyzed. Positive immunostaining for Tbr2 was observed, confined mainly to the ventricular and subventricular zone, where 58.21 ± 1.71% of SVCT2-eGFP cells co-localized with anti-Tbr2 (Figure 6c,e). However, in the different layers of the cerebral cortex, there was no positive labeling for Tbr2 since IPs do not localize in these areas. Therefore, given that Tbr2 presents a neuronal lineage and, that some SVCT2-eGFP cells from the V-SVZ and inner region of the intermediate zone co-localize with it, we hypothesized that the SVCT2-eGFP cells that migrated to the different layers of the cerebral cortex correspond to immature neurons.

A second analysis was conducted with the antibody doublecortin (DCX), a microtubule-associated protein expressed in migrating neurons (Gleeson et al., 1999), and with the astrocyte marker, GFAP. The results showed prominent co-localization between SVCT2-eGFP-positive cells with the DCX marker and little or no co-localization with the GFAP marker (Figure 6d). Notably, it was quantitatively determined that 84.8 ± 7.18% of SVCT2-eGFP positive cells co-localized with DCX (Figure 6e). In contrast, 0.85 ± 0.54% of SVCT2-eGFP positive cells were visualized co-localizing with the GFAP marker (Figure 6e). Accordingly, the compilation of these data provided evidence that overexpression of SVCT2 in cells of the ventricular region leads to differentiation of IRG cells into a neuronal lineage.

3.7 | Modulation of signaling pathways by SVCT2

To determine whether different levels of SVCT2 lead to an increase or decrease in neuronal (NeuN and βIII-tubulin) or astrocytic (GFAP) markers, protein extracts obtained from the cortex of 1-day postnatal SVCT2^{wt}, SVCT2$^{+/-}$ and SVCT2^{tg} mice were analyzed by western blot (Figure 7a). The AA content was analyzed in the cortex/hindbrain, and as expected, a decrease of AA in tissues from SVCT2$^{+/-}$ mice and an increase of AA in tissues from SVCT2^{tg} mice when compared to the control was determined (Figure S5a). Interestingly, when using the mature neuron marker, anti-NeuN, it was observed that the ~50 kDa immunoreactive band was significantly increased in SVCT2^{tg} mice, with ~twofold greater intensity than the control group, while in the SVCT2$^{+/-}$ mice, a slightly, but not significant decrease in band intensity was observed (Figure 7c). However, NeuN abundance in SVCT2$^{+/-}$ mice cortex was significantly lower than in SVCT2^{tg} mice (Figure 7c). When analyzing βIII-tubulin levels, it was obtained that the SVCT2^{tg} mice exhibited a robust and significant accumulation in the ~55 kDa immunoreactive band, whose levels were double with respect to the SVCT2^{wt} (Figure 7e), and around 5-fold higher compared to SVCT2$^{+/-}$ mice group (Figure 7e). On the other hand, although it was observed that the SVCT2$^{+/-}$ mice presented a lower abundance in the ~55 kDa immunoreactive band with respect to the control, this decrease was not significant (Figure 7e). This pattern was strongly reversed when an anti-GFAP antibody was used, where in this case, the accumulation of the ~50 kDa immunoreactive band was preferentially enriched in the SVCT2$^{+/-}$ mice (Figure 7d), increasing significantly ~2-fold with respect to the control group (Figure 7d). For its part, the SVCT2^{tg} group exhibited a significant decrease in GFAP, with respect to the control condition (Figure 7d).

Finally, to gain insights into the potential mechanisms by which different levels of SVCT2 and therefore AA, can regulate the differentiation of neural precursors, we evaluated different mediators that have been previously shown to have a role during cortical development, including AKT, GSK3-β, p44/42 MAPK (ERK1/2) or mTOR (Andrews et al., 2020; Kim et al., 2009; Wang et al., 2016; Zhang et al., 2013). In this regard, protein lysates obtained from the cerebral cortex of SVCT2^{wt}, SVCT2$^{+/-}$, or SVCT2^{tg} mice at P1 were subjected to western blot analyses (Figure 7b). First, we evaluated the levels of phosphorylated AKT at Ser473 (AKT-Ser473), which corresponds to an active form of AKT (Sarbassov et al., 2005). Our data showed that the levels of SVCT2 directly regulate the phosphorylation status of AKT at Ser473 (Figure 7b,f). On one hand, SVCT2$^{+/-}$ mice exhibited increased levels of AKT-Ser473 compared to SVCT2^{WT} mice by ~1.5

FIGURE 6 Analysis of SVCT2 overexpression in IRG cells in 1-day postnatal rat brains. (a) Electroporated cells with SVCT2-eGFP or eGFP-positive and nuclei were visualized with Höechst (blue). Yellow dotted lines highlight the location of SVCT2-eGFP-positive cells at different stages post-electroporation and white dotted lines delimit the VZ-SVZ of the lateral ventricle. Some radial processes and endfoot of IRG cells observed in eGFP-positive cells are indicated by arrows and white arrowheads, respectively. Higher magnification of cell morphology at 2 days post-electroporation (white boxes) are shown in (i) and (ii) (b) Confocal microscopy analysis of frontal slices of brains injected intraventricularly with BrdU and SVCT2-eGFP plasmid at 1-day postnatal stage and analyzed 2 days post-electroporation. SVCT2-eGFP-positive cells are shown in green and BrdU-positive cells are distinguished in red. (c) Representative immunohistochemical images of rat brains electroporated with SVCT2-eGFP at 1-day postnatal stage and sacrificed at 2 days postnatal, immunoreaction for the intermediate progenitor marker, Tbr2 (red) and SVCT2-eGFP (green). Higher magnification of co-localization (white boxes) between SVCT2-eGFP-positive cells and Tbr2 are shown in (i), (ii) and (iii) (d) Confocal microscopy analysis of rat brains electroporated with SVCT2-eGFP at 1 day postnatal and visualized at 7 days post-electroporation. For the neuronal migration protein, doublecortin (red), GFAP (white), and SVCT2-eGFP (green) (i–iii). Digitally enhanced images of boxes i-iii. (e) Quantitative analysis of the SVCT2-eGFP-positive cells that co-localize with anti-BrdU, anti-Tbr2, and anti-DCX signals. In all images, nuclei were observed with Höechst (blue). LV, lateral ventricle; VZ, ventricular zone; PS, pial surface. Scale bar: 50 μm (a–d).

10981136, 0, Downloaded from https://onlinelibrary.wiley.com/doi/10.1002/glia.24498 by Chuar-Consorcio De Bibliotecas, Wiley Online Library on [26/01/2024]. See the Terms and Conditions (https://onlinelibrary.wiley.com/terms-and-conditions) on Wiley Online Library for rules of use; OA articles are governed by the applicable Creative Commons License

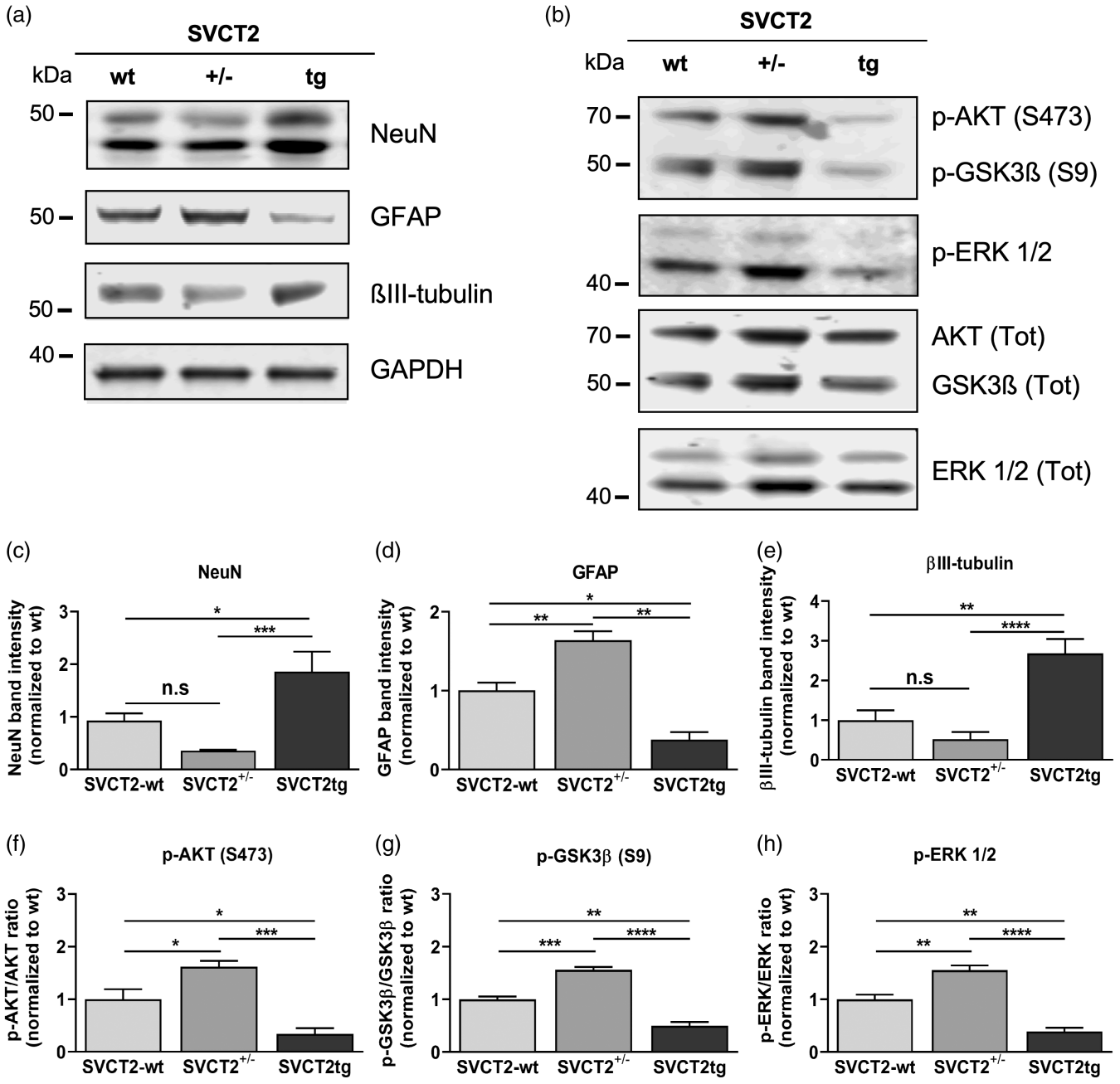

FIGURE 7 Analysis of neuronal and astrocytic markers along with the effectors AKT, GSK3, and ERK in the cerebral cortex of 1-day postnatal mice. (a) Western blots performed against anti-NeuN, anti-GFAP, and βIII-tubulin, whose levels were normalized with respect to GAPDH on protein extracts collected from the cerebral cortex of $SVCT2^{wt}$, $SVCT2^{+/-}$ or $SVCT2^{tg}$ mice. (b) Western blots performed against phosphorylated ERK 1/2, AKT (Ser473), and GSK3β (Ser9) and their respective non-phosphorylated forms. (c–h) The intensity of the different bands was quantified by ImageJ and normalized with respect to $SVCT2^{wt}$ values and subsequently plotted as the mean ± SEM for each condition. Statistical analyses were performed by using one-way ANOVA (F-value = 51.57 for NeuN; $F = 18.34$ for βIII-tubulin; $F = 35.79$ for GFAP; $F = 22.39$ for AKT; $F = 81.54$ for GSK3β and $F = 55.01$ for ERK) followed by Tukey's post hoc multiple comparison test. $^{****}p < 0.0001$; $^{***}p < 0.001$: $^{**}p < 0.01$; $^{*}p < 0.05$; n.s for $p > 0.05$. $n = 3$.

fold (Figure 7b,f), whereas SVCT2-tg mice displayed a sharp decrease in the abundance of active AKT (Figure 7f). Similarly, the direct downstream target of AKT-Ser473, GSK3-β, which is inactivated by phosphorylation at Serine-9 and has been proposed as a regulator of neural progenitor homeostasis (Kim et al., 2009), was found with the lowest degree of phosphorylation (i.e., high active state) in the $SVCT2^{tg}$ mice and conversely, with the highest level of phosphorylation in $SVCT2^{+/-}$ mice (Figure 7b,g). We also evaluated the potential regulation of SVCT2 upstream of AKT. Considering that phosphorylation of AKT at Ser473 or Thr308 can be used as a readout of mTOR-C2 or PI3K/PDK1 signaling activity, respectively (Alessi et al., 1996; Saxton & Sabatini, 2017; Zhang et al., 2013), we analyzed

10981136, 0, Downloaded from https://onlinelibrary.wiley.com/doi/10.1002/glia.24498 by Cbua-Consorcio De Bibliotecas, Wiley Online Library on [26/01/2024]. See the Terms and Conditions (https://onlinelibrary.wiley.com/terms-and-conditions) on Wiley Online Library for rules of use; OA articles are governed by the applicable Creative Commons License

the levels of phosphorylated mTORC2 and PDK1, where we observed that the levels of these effectors were differentially modulated by SVCT2 levels, where higher levels of phosphorylation of mTORC2 and PDK1 were found in SVCT2$^{+/-}$ mice (Figure S5b).

On the other hand, we also evaluated the effect of SVCT2 levels on the activation of ERK1/2 signaling. In this context, our data showed that ERK1/2 phosphorylation was significantly decreased in the SVCT2^{tg} mice, whereas SVCT2$^{+/-}$ mice exhibited an increase in the levels of phospho-ERK (Figure 7b,h). Collectively, these data indicate that SVCT2 is regulating signaling pathways that mediate cortical development.

4 | DISCUSSION

Notwithstanding that we found a considerable number of lRG cells in the postnatal brain, it is likely that not all lRG cells retain their stem cell characteristics. Previous studies have shown that embryonic RG cells are specified in the ependymal lineage between E14 and E16; therefore, they undergo their last division in these embryonic periods (Kyrousi et al., 2017). Nevertheless, and curiously, they maintain their morphological and glial characteristics until birth (Kyrousi et al., 2017). Similarly, the majority of mouse B1 cell precursors are produced from embryonic RG cells present at E13.5–E15.5 and remain quiescent until reactivation at the adult stage (Fuentealba et al., 2015). Further, the embryonic RG cells progressively restrict their differentiation potential; projection neurons are generated in successive waves in an inside-out patterning, and then, glial cells are produced (Kriegstein & Alvarez-Buylla, 2009; Qian et al., 2000; Temple, 2001). Consequently, although lRG cells are highly present in the first postnatal days preserving their morphology, a number of these cells must have lost their proliferative capacity, and/or their differentiation potential is probably restricted to the generation of glial cells. However, we observed Sox2 and BrdU positive cells labeling at the dorsal VZ/SVZ of the lateral ventricles. Thus, it is likely that in early postnatal stages (PN1-4), an undifferentiated and proliferative subpopulation of lRG cells persists in the dorsal region of lateral ventricles, where the greatest amount of elongated radial processes, which had contact with the VZ and the pial surface were distinguished.

During the development of the mammalian brains, neurons, and glial cells are generated in an orderly sequence with neurogenesis preceding gliogenesis, where the neurogenic-to-gliogenic transition occurs between E12 and E16 (La Manno et al., 2021). After that period, embryonic RG cells start to disappear becoming astrocytes or generating ependymal or, in adult stages, B1 cells (Kriegstein & Alvarez-Buylla, 2009). It is worth mentioning that other research groups have determined the postnatal generation of neurons from the SVZ. For instance, from the SVZ in early postnatal stages, the generation of GABAergic interneurons (Inta et al., 2008), and of a class of neurons called "small axonless neurons", which were preferentially located in the deeper layers of the orbital and olfactory cortex, have been described (Le Magueresse et al., 2011). Instead, in this work, eGFP+ cells exhibiting a migratory neuronal morphology were in cortical layers II/III and, given that their migration was radial and not tangential, it is likely these labeled cells correspond to pyramidal neurons. However, further studies are required to determine the exact neuronal identity. Also, it is feasible that our adenovirus labeling only transduced a specific population of lRG cells, and that the generation of neurons from lRG cells is possibly well below glial production.

To our knowledge, to date, there are no known factors or molecules that may be regulating lRG cells differentiation. In this context, AA, and its transporter SVCT2 could be feasible candidates. Compelling evidence suggests that AA enters the CSF through the choroid plexuses, which have a basolaterally polarized SVCT2 transporter (Ulloa et al., 2013; Ulloa et al., 2019). Our analyses revealed that SVCT2 is highly polarized in the apical region of lRG cells, which has contact with CSF, suggesting that AA is uptake by this neural stem cell. Concordant with these results, it has been demonstrated the ventricular polarization of SVCT2 in embryonic rat (Caprile et al., 2009) as well as, mouse and human brains, which co-localizes with RG markers (Silva-Alvarez et al., 2016). However, although several investigations of SVCT2 and AA, including this work, have used rat and mouse models interchangeably, it is not known whether there are differences in the SVCT2 expression/function between rat and mouse, which could clearly impact the interpretation of our results.

Our functional analysis showed that AA and SVCT2 in vitro would maintain the undifferentiated state of lRG-like cells, meanwhile promoting neurogenic differentiation in vivo. The existence of dual effects of AA in stem cell differentiation has been widely demonstrated in the literature. On the one hand, our laboratory and other research groups have shown its neurogenic role (Espinoza et al., 2020; Han et al., 2021; Jara et al., 2022; Oyarce et al., 2018; Pastor et al., 2013; Shin et al., 2004; Yan et al., 2001). Furthermore, in the cerebral cortex of SVCT2$^{+/-}$ mice, there is 30%–40% less AA than in normal brains (Dixit et al., 2015; Meredith & May, 2013). These mice showed moderate hyperactivity, impaired motor coordination and balance, as well as decreased spatial memory (Dixit et al., 2015). In this regard, spatial memory is a hippocampal-dependent task (Fritch et al., 2020), and it has been determined that embryonic hippocampal neurons from SVCT2$^{-/-}$ mice exhibit a lower amplitude and frequency of mEPCs as well as a lower number and length of dendrites, in addition to a decrease in the number of GLUR1 glutamate receptors (Qiu et al., 2007). Relatedly, research in SVCT2$^{-/-}$, SVCT2$^{+/-}$, and SVCT2^{wt} mice analyzed the number of embryonic dopaminergic neurons at the mesencephalic level. Histologic counting showed a marked decrease of TH+ dopaminergic neuron formation in the knockout embryos in an *Svct2* dose-dependent manner (He et al., 2015), indicating that decreased levels of SVCT2 translate into a lower rate of neurogenesis. The above agrees with our results, where we determined that the cerebral cortex of mice with low levels of SVCT2 presents a significantly lower abundance of neuronal markers (NeuN and βIII-tubulin), which is reversed when analyzing the cerebral cortex presenting with high levels of SVCT2. It is plausible that in vivo overexpression of SVCT2 in lRG cells will indirectly potentiate their differentiation into neurons by generating intermediate progenitors or directly by differentiating into neuroblasts. On the other hand, it has

10981136, 0, Downloaded from https://onlinelibrary.wiley.com/doi/10.1002/glia.24498 by Chun-Consorcio De Bibliotecas, Wiley Online Library on [26/01/2024]. See the Terms and Conditions (https://onlinelibrary.wiley.com/terms-and-conditions) on Wiley Online Library for rules of use; OA articles are governed by the applicable Creative Commons License

been reported that AA increases the levels of Nanog, a key transcription factor in maintaining the undifferentiated state of stem cells (Wu et al., 2014) and blocking differentiation (Pan & Thomson, 2007). In this context, AA treatment maintained the undifferentiated state and enhanced self-renewal in the J1 cell line (Gao et al., 2013). Furthermore, it has been determined that AA, independent of its antioxidant activity, increases the generation of induced pluripotent stem cells (iPSCs) in both human and mouse (Esteban et al., 2010). Simultaneously, other studies have shown that the addition of AA to the culture media of somatic cells (during reprogramming) improves the efficiency, maintenance, and proliferation of iPSCs (Stadtfeld et al., 2012; Wang et al., 2011). In this sense, it is well established that AA has dual roles, participating in maintaining the undifferentiated state or in neurogenic differentiation in embryonic and adult brains and in cellular models in vitro (Salazar et al., 2023). It is reasonable to assume that the role of AA depends on the cell type, the cellular context, the time in which it is involved, and the signaling pathways involved. Interestingly, it has been proposed that SVCT2 constitutively interacts with JAK2 and mediates the activation of the JAK2/STAT2 signaling cascade, which would be induced by AA (Han et al., 2021). In this respect, Salazar et al. demonstrated that overexpression of SVCT2 in the neuroblastoma cell line N2a induced neuronal differentiation. Notably, neither AA supplementation nor SVCT1 reproduced the morphological changes caused by SVCT2 overexpression (Salazar et al., 2016). Therefore, while it is likely that in vivo SVCT2 overexpression increased the uptake of AA by IRG cells and consequently leads to neuronal differentiation, further studies are required to determine whether the observed effect is a result of AA and/or SVCT2.

The signaling pathways that AA may regulate in neural stem cell pluripotency/differentiation remain poorly understood. Our data indicated that in brains that have high levels of SVCT2/AA, where higher levels of neuronal markers (NeuN and ß-III tubulin) were observed, AKT pathway is inhibited. It has been previously described that upon inhibition of AKT in embryonic RG cells, there was an increased cell exit from the VZ toward the pial surface and premature neuronal differentiation (Zhang et al., 2013). In line with this notion, enhanced AKT activation in vivo promoted the retention of embryonic RG cells in the V-SVZ, and in vitro, promoted a stem cell state (Sinor & Lillien, 2004). Although in this work we did not elucidate which effectors upstream of AKT are modulated by AA and/or SVCT2, other authors have established that AA down-regulated IGF-1R as well as the activity of PI3K/AKT, MAPK/ERK, and mTOR signaling (Lee et al., 2008; Qin et al., 2023; Su et al., 2019). Therefore, it is likely that when we overexpressed SVCT2 in the IRG cells in vivo, mTORC2 and PDK1 were inactivated and unable to phosphorylate AKT, and therefore GSK3-β is activated, thus promoting the generation of migratory neurons. In general, AKT inhibits GSK3-β by S9 phosphorylation leading to inactivation because the N-terminus of GSK3-β competitively blocks substrate docking in the primed substrate pocket (Frame et al., 2001). Our result showed that in mice with higher levels of SVCT2, GSK3-β had the lowest degree of S9 phosphorylation and therefore, a higher activate state, probably because AKT is found less active in these mice. In this sense, it has been proposed that GSK3-β deletion removes homeostatic controls on neural progenitors, shifting the balance toward self-renewal, massively expanding the radial progenitor pool, and leading away from neurogenesis (Kim et al., 2009). Unexpectedly, we found that the ERK1/2 pathway was decreased in brains with high levels of SVCT2 although it has been shown that overexpression of SVCT2 and treatment with AA promoted ERK1/2 phosphorylation, stimulating neuronal differentiation (Li et al., 2006; Salazar et al., 2016; Semprich et al., 2022). However, it has also been demonstrated that ERK1/2 inhibits neuronal differentiation of neural stem cells (Wang et al., 2009) and upregulates the expression of astrocyte-related genes (Wang et al., 2016). Strikingly, unpublished data showed that high-dose of AA resulted in persistent ERK feedback inhibition following activation (https://doi.org/10.1101/2022.01.11.475954), and this may explain why we observed a decrease of p-ERK1/2 in brains with high levels of SVCT2/AA. However, although we have elucidated a possible signaling pathway involved, it does not explain why SVCT2 and/or AA have distinct in vitro and in vivo effects on IRG cells. We consider that in situ, there are other factors that converge the response and activate/inactivate signaling pathways of IRG cells to AA. Therefore, it is likely that in vivo overexpression of SVCT2 generates activation of the AKT pathway and inhibits, by an as-yet-unknown pathway, the pluripotency signaling pathway, due to the presence of other factors that condition the response, e.g., retinoic acid from the meninges which are not present in vitro. A potential candidate could be JAK2/STAT2/nanog signaling which AA/SVCT2 is known to activate in vitro (Han et al., 2021; Wu et al., 2014). In summary, AA can activate the JAK/STAT2/nanog signaling pathways and AKT. Because these signaling pathways crosstalk, AKT inhibiting JAK/STAT (Kang et al., 2018), the final response of IRG cells will depend on other factors that regulate the predominant pathway of activation. Undoubtedly, further studies are needed to confirm this hypothesis.

AUTHOR CONTRIBUTIONS

Natalia Saldivia, Katterine Salazar, Manuel Cifuentes, Francisca Espinoza, Fiona E. Harrison, and Francisco Nualart conducted experiments. Natalia Saldivia, Katterine Salazar, and Manuel Cifuentes performed the experiments. Natalia Saldivia, Katterine Salazar, Manuel Cifuentes, Fiona E. Harrison, and Francisco Nualart analyzed the data. Natalia Saldivia and Francisco Nualart wrote the article. Natalia Saldivia, Katterine Salazar, Manuel Cifuentes, Francisca Espinoza, Fiona E. Harrison, and Francisco Nualart critically revised the manuscript. All authors approved the final version of the manuscript.

ACKNOWLEDGMENTS

This work was funded by grants FONDECYT 1221147 to FN, CONICYT-PIA ECM-12 to FN, and Fondecyt 1190848 to KS. The authors thank Ximena Koch from Universidad de Concepción for her technical assistance in the histological handling, and Adriana Tienda from Vanderbilt University Medical Center, for her help with acquiring the tissues and determination of AA content. The funders had no role in the study.

10981136, 0, Downloaded from https://onlinelibrary.wiley.com/doi/10.1002/glia.24498 by Chun-Consorcio De Bibliotecas, Wiley Online Library on [26/01/2024]. See the Terms and Conditions (https://onlinelibrary.wiley.com/terms-and-conditions) on Wiley Online Library for rules of use; OA articles are governed by the applicable Creative Commons License

CONFLICT OF INTEREST STATEMENT

No potential conflicts of interest relevant to this article were reported.

DATA AVAILABILITY STATEMENT

Primary data and materials described are available on request for academic use.

ORCID

Francisco Nualart https://orcid.org/0000-0002-7762-1417

REFERENCES

Alessi, D. R., Andjelkovic, M., Caudwell, B., Cron, P., Morrice, N., Cohen, P., & Hemmings, B. A. (1996). Mechanism of activation of protein kinase B by insulin and IGF-1. *The EMBO Journal*, *15*(23), 6541–6551.

Andrews, M. G., Subramanian, L., & Kriegstein, A. R. (2020). mTOR signaling regulates the morphology and migration of outer radial glia in developing human cortex. *eLife*, *9*, 9.

Astuya, A., Caprile, T., Castro, M., Salazar, K., García, M. A., Reinicke, K., Rodríguez, F., Vera, J. C., Millán, C., Ulloa, V., Low, M., Martínez, F., & Nualart, F. (2005). Vitamin C uptake and recycling among normal and tumor cells from the central nervous system. *Journal of Neuroscience Research*, *79*(1–2), 146–156.

Baeza, V., Cifuentes, M., Martínez, F., Ramírez, E., Nualart, F., Ferrada, L., Oviedo, M. J., de Lima, I., Troncoso, N., Saldivia, N., & Salazar, K. (2021). IIIG9 inhibition in adult ependymal cells changes adherens junctions structure and induces cellular detachment. *Scientific Reports*, *11*(1), 18537.

Bodannes, R. S., & Chan, P. C. (1979). Ascorbic acid as a scavenger of singlet oxygen. *FEBS Letters*, *105*(2), 195–196.

Caprile, T., Salazar, K., Astuya, A., Cisternas, P., Silva-Alvarez, C., Montecinos, H., Millán, C., García, M. A., & Nualart, F. (2009). The Na+−dependent L-ascorbic acid transporter SVCT2 expressed in brainstem cells, neurons, and neuroblastoma cells is inhibited by flavonoids. *Journal of Neurochemistry*, *108*(3), 563–577.

Dixit, S., Bernardo, A., Walker, J. M., Kennard, J. A., Kim, G. Y., Kessler, E. S., & Harrison, F. E. (2015). Vitamin C deficiency in the brain impairs cognition, increases amyloid accumulation and deposition, and oxidative stress in APP/PSEN1 and normally aging mice. *ACS Chemical Neuroscience*, *6*(4), 570–581.

Dixit, S., Fessel, J. P., & Harrison, F. E. (2017). Mitochondrial dysfunction in the APP/PSEN1 mouse model of Alzheimer's disease and a novel protective role for ascorbate. *Free Radical Biology & Medicine*, *112*, 515–523.

Espinoza, F., Magdalena, R., Saldivia, N., Jara, N., Martínez, F., Ferrada, L., Salazar, K., Ávila, F., & Nualart, F. (2020). Vitamin C recycling regulates neurite growth in Neurospheres differentiated in vitro. *Antioxidants (Basel)*, *9*(12), 1276–1293.

Esteban, M. A., Wang, T., Qin, B., Yang, J., Qin, D., Cai, J., Li, W., Weng, Z., Chen, J., Ni, S., Chen, K., Li, Y., Liu, X., Xu, J., Zhang, S., Li, F., He, W., Labuda, K., Song, Y., … Pei, D. (2010). Vitamin C enhances the generation of mouse and human induced pluripotent stem cells. *Cell Stem Cell*, *6*(1), 71–79.

Ferrada, L., Barahona, M. J., Salazar, K., Vandenabeele, P., & Nualart, F. (2020). Vitamin C controls neuronal necroptosis under oxidative stress. *Redox Biology*, *29*, 101408.

Ferrada, L., Magdalena, R., Barahona, M. J., Ramírez, E., Sanzana, C., Gutiérrez, J., & Nualart, F. (2021). Two distinct faces of vitamin C: AA vs. DHA. *Antioxidants (Basel)*, *10*(2), 215–231.

Frame, S., Cohen, P., & Biondi, R. M. (2001). A common phosphate binding site explains the unique substrate specificity of GSK3 and its inactivation by phosphorylation. *Molecular Cell*, *7*(6), 1321–1327.

Fritch, H. A., MacEvoy, S. P., Thakral, P. P., Jeye, B. M., Ross, R. S., & Slotnick, S. D. (2020). The anterior hippocampus is associated with spatial memory encoding. *Brain Research*, *1732*, 146696.

Fuentealba, L. C., Rompani, S. B., Parraguez, J. I., Obernier, K., Romero, R., Cepko, C. L., & Alvarez-Buylla, A. (2015). Embryonic origin of postnatal neural stem cells. *Cell*, *161*(7), 1644–1655.

Furutachi, S., Miya, H., Watanabe, T., Kawai, H., Yamasaki, N., Harada, Y., Imayoshi, I., Nelson, M., Nakayama, K. I., Hirabayashi, Y., & Gotoh, Y. (2015). Slowly dividing neural progenitors are an embryonic origin of adult neural stem cells. *Nature Neuroscience*, *18*(5), 657–665.

Gao, Y., Yang, L., Chen, L., Wang, X., Wu, H., Ai, Z., du, J., Liu, Y., Shi, X., Wu, Y., Guo, Z., & Zhang, Y. (2013). Vitamin C facilitates pluripotent stem cell maintenance by promoting pluripotency gene transcription. *Biochimie*, *95*(11), 2107–2113.

García, M. A., Salazar, K., Millán, C., Rodríguez, F., Montecinos, H., Caprile, T., Silva, C., Cortes, C., Reinicke, R., Vera, J. C., Aguayo, L. G., Olate, J., Molina, B., & Nualart, F. (2005). Sodium vitamin C cotransporter SVCT2 is expressed in hypothalamic glial cells. *Glia*, *50*(1), 32–47.

Glaser, T., & Brustle, O. (2005). Retinoic acid induction of ES-cell-derived neurons: The radial glia connection. *Trends in Neurosciences*, *28*(8), 397–400.

Gleeson, J. G., Lin, P. T., Flanagan, L. A., & Walsh, C. A. (1999). Doublecortin is a microtubule-associated protein and is expressed widely by migrating neurons. *Neuron*, *23*(2), 257–271.

Han, Z., Zhang, Z., Guan, Y., Chen, B., Yu, M., Zhang, L., Fang, J., Gao, Y., & Guo, Z. (2021). New insights into vitamin C function: Vitamin C induces JAK2 activation through its receptor-like transporter SVCT2. *International Journal of Biological Macromolecules*, *173*, 379–398.

Harrison, F. E., Best, J. L., Meredith, M. E., Gamlin, C. R., Borza, D. B., & May, J. M. (2012). Increased expression of SVCT2 in a new mouse model raises ascorbic acid in tissues and protects against paraquat-induced oxidative damage in lung. *PLoS One*, *7*(4), e35623.

Harrison, F. E., & May, J. M. (2009). Vitamin C function in the brain: Vital role of the ascorbate transporter SVCT2. *Free Radical Biology & Medicine*, *46*(6), 719–730.

He, X. B., Kim, M., Kim, S. Y., Yi, S. H., Rhee, Y. H., Kim, T., Lee, E. H., Park, C. H., Dixit, S., Harrison, F. E., & Lee, S. H. (2015). Vitamin C facilitates dopamine neuron differentiation in fetal midbrain through TET1- and JMJD3-dependent epigenetic control manner. *Stem Cells*, *33*(4), 1320–1332.

Hevner, R. F. (2019). Intermediate progenitors and Tbr2 in cortical development. *Journal of Anatomy*, *235*(3), 616–625.

Inta, D., Alfonso, J., von Engelhardt, J., Kreuzberg, M. M., Meyer, A. H., van Hooft, J. A., & Monyer, H. (2008). Neurogenesis and widespread forebrain migration of distinct GABAergic neurons from the postnatal subventricular zone. *Proceedings of the National Academy of Sciences of the United States of America*, *105*(52), 20994–20999.

Jara, N., Cifuentes, M., Martínez, F., González-Chavarría, I., Salazar, K., Ferrada, L., & Nualart, F. (2022). Vitamin C deficiency reduces neurogenesis and proliferation in the SVZ and lateral ventricle extensions of the Young Guinea pig brain. *Antioxidants (Basel)*, *11*(10), 2030–2041.

Jones-Villeneuve, E. M., Rudnicki, M. A., Harris, J. F., & McBurney, M. (1983). Retinoic acid-induced neural differentiation of embryonal carcinoma cells. *Molecular and Cellular Biology*, *3*(12), 2271–2279.

Kang, D., Wang, D., Xu, J., Quan, C., Guo, X., Wang, H., Luo, J., Yang, Z., Chen, S., & Chen, J. (2018). The InR/Akt/TORC1 growth-promoting signaling negatively regulates JAK/STAT activity and migratory cell fate during morphogenesis. *Developmental Cell*, *44*(4), 524–531 e5.

Kim, W. Y., Wang, X., Wu, Y., Doble, B. W., Patel, S., Woodgett, J. R., & Snider, W. D. (2009). GSK-3 is a master regulator of neural progenitor homeostasis. *Nature Neuroscience*, *12*(11), 1390–1397.

Kosodo, Y., & Huttner, W. B. (2009). Basal process and cell divisions of neural progenitors in the developing brain. *Development, Growth & Differentiation*, *51*(3), 251–261.

10981136, 0, Downloaded from https://onlinelibrary.wiley.com/doi/10.1002/glia.24498 by Chun-Consorcio De Bibliotecas, Wiley Online Library on [26/01/2024]. See the Terms and Conditions (https://onlinelibrary.wiley.com/terms-and-conditions) on Wiley Online Library for rules of use; OA articles are governed by the applicable Creative Commons License

Kriegstein, A., & Alvarez-Buylla, A. (2009). The glial nature of embryonic and adult neural stem cells. *Annual Review of Neuroscience*, *32*, 149–184.

Kyrousi, C., Lygerou, Z., & Taraviras, S. (2017). How a radial glial cell decides to become a multiciliated ependymal cell. *Glia*, *65*(7), 1032–1042.

La Manno, G., Siletti, L., Furlan, A., Gyllborg, D., Vinsland, E., Mossi Albiach, A., Mattsson Langseth, Ch., Khven, I., Lederer, A. R., Dratva, L. M., Johnsson, A., Nilsson, M., Lönnerberg, P., & Linnarsson, S. (2021). Molecular architecture of the developing mouse brain. *Nature*, *596*(7870), 92–96.

Le Magueresse, C., Alfonso, J., Khodosevich, K., Arroyo Martín, A. A., Bark, Ch. & Monyer, H. (2011). "small axonless neurons": Postnatally generated neocortical interneurons with delayed functional maturation. *The Journal of Neuroscience*, *31*(46), 16731–16747.

Lee, J. Y., Chang, M. Y., Park, C. H., Kim, H. Y., Kim, J. H., Son, H., Lee, Y. S., & Lee, S. H. (2003). Ascorbate-induced differentiation of embryonic cortical precursors into neurons and astrocytes. *Journal of Neuroscience Research*, *73*(2), 156–165.

Lee, S. K., Kang, J. S., Jung, D. J., Hur, D. Y., Kim, J. E., Hahm, E., Bae, S., Kim, H. W., Kim, D., Cho, B. J., Cho, D., Shin, D. H., Hwang, Y. I., & Lee, W. J. (2008). Vitamin C suppresses proliferation of the human melanoma cell SK-MEL-2 through the inhibition of cyclooxygenase-2 (COX-2) expression and the modulation of insulin-like growth factor II (IGF-II) production. *Journal of Cellular Physiology*, *216*(1), 180–188.

Li, Z., Theus, M. H., & Wei, L. (2006). Role of ERK 1/2 signaling in neuronal differentiation of cultured embryonic stem cells. *Development, Growth & Differentiation*, *48*(8), 513–523.

Martinez, F., Cifuentes, M., Tapia, J. C., & Nualart, F. (2019). The median eminence as the hypothalamic area involved in rapid transfer of glucose to the brain: Functional and cellular mechanisms. *Journal of Molecular Medicine (Berlin, Germany)*, *97*(8), 1085–1097.

Meredith, M. E., Harrison, F. E., & May, J. M. (2011). Differential regulation of the ascorbic acid transporter SVCT2 during development and in response to ascorbic acid depletion. *Biochemical and Biophysical Research Communications*, *414*(4), 737–742.

Meredith, M. E., & May, J. M. (2013). Regulation of embryonic neurotransmitter and tyrosine hydroxylase protein levels by ascorbic acid. *Brain Research*, *1539*, 7–14.

Merkle, F. T., Tramontin, A. D., García-Verdugo, J. M., & Alvarez-Buylla, A. (2004). Radial glia give rise to adult neural stem cells in the subventricular zone. *Proceedings of the National Academy of Sciences of the United States of America*, *101*(50), 17528–17532.

Mori, T., Buffo, A., & Gotz, M. (2005). The novel roles of glial cells revisited: The contribution of radial glia and astrocytes to neurogenesis. *Current Topics in Developmental Biology*, *69*, 67–99.

Mun, G. H., Kim, M. J., Lee, J. H., Kim, H. J., Chung, Y. H., Chung, Y. B., Kang, J. S., Hwang, Y. I., Oh, S. H., Kim, J. G., Hwang, D. H., Shin, D. H., & Lee, W. J. (2006). Immunohistochemical study of the distribution of sodium-dependent vitamin C transporters in adult rat brain. *Journal of Neuroscience Research*, *83*(5), 919–928.

Noctor, S. C., Flint, A. C., Weissman, T. A., Wong, W. S., Clinton, B. K., & Kriegstein, A. R. (2002). Dividing precursor cells of the embryonic cortical ventricular zone have morphological and molecular characteristics of radial glia. *The Journal of Neuroscience*, *22*(8), 3161–3173.

Nualart, F., Salazar, K., Oyarce, K., Cisternas, P., Jara, N., Silva-Álvarez, C., Pastor, P., Martínez, F., García, A., García-Robles, M. Á., & Tapia, J. C. (2012). Typical and atypical stem cells in the brain, vitamin C effect and neuropathology. *Biological Research*, *45*(3), 243–256.

Nualart, F., Mack, L., García, A., Cisternas, P., Bongarzone, E. R., Heitzer, M., Jara, N., Martínez, F., Ferrada, L., Espinoza, F., Baeza, V., & Salazar, K. (2014). Vitamin C transporters, recycling and the bystander effect in the nervous system: SVCT2 versus gluts. *Stem Cell Research & Therapy*, *4*(5), 209.

Ortiz-Alvarez, G., & Spassky, N. (2021). One progenitor to generate them all: New evidence for multi-fated neural progenitors. *Current Opinion in Neurobiology*, *66*, 186–194.

Oyarce, K., Silva-Alvarez, C., Ferrada, L., Martínez, F., Salazar, K., & Nualart, F. (2018). SVCT2 is expressed by cerebellar precursor cells, which differentiate into neurons in response to ascorbic acid. *Molecular Neurobiology*, *55*(2), 1136–1149.

Pan, G., & Thomson, J. A. (2007). Nanog and transcriptional networks in embryonic stem cell pluripotency. *Cell Research*, *17*(1), 42–49.

Pastor, P., Cisternas, P., Salazar, K., Silva-Alvarez, C., Oyarce, K., Jara, N., Espinoza, F., Martínez, A. D., & Nualart, F. (2013). SVCT2 vitamin C transporter expression in progenitor cells of the postnatal neurogenic niche. *Frontiers in Cellular Neuroscience*, *7*, 119.

Pebworth, M. P., Ross, J., Andrews, M., Bhaduri, A., & Kriegstein, A. R. (2021). Human intermediate progenitor diversity during cortical development. *Proceedings of the National Academy of Sciences of the United States of America*, *118*(26), e2019415118.

Portugal, C. C., Socodato, R., Canedo, T., Silva, C. M., Martins, T., Coreixas, V. S. M., Loiola, E. C., Gess, B., Röhr, D., Santiago, A. R., Young, P., Minshall, R. D., Paes-de-Carvalho, R., Ambrósio, A. F., & Relvas, J. B. (2017). Caveolin-1-mediated internalization of the vitamin C transporter SVCT2 in microglia triggers an inflammatory phenotype. *Science Signaling*, *10*(472), eaal2005.

Qian, X., Shen, Q., Goderie, S. K., He, W., Capela, A., Davis, A. A., & Temple, S. (2000). Timing of CNS cell generation: A programmed sequence of neuron and glial cell production from isolated murine cortical stem cells. *Neuron*, *28*(1), 69–80.

Qin, S., Wang, G., Chen, L., Geng, H., Zheng, Y., Xia, C., Wu, S., Yao, J., & Deng, L. (2023). Pharmacological vitamin C inhibits mTOR signaling and tumor growth by degrading Rictor and inducing HMOX1 expression. *PLoS Genetics*, *19*(2), e1010629.

Qiu, S., Li, L., Weeber, E. J., & May, J. M. (2007). Ascorbate transport by primary cultured neurons and its role in neuronal function and protection against excitotoxicity. *Journal of Neuroscience Research*, *85*(5), 1046–1056.

Redmond, S. A., Figueres-Oñate, M., Obernier, K., Nascimento, M. A., Parraguez, J. I., López-Mascaraque, L., Fuentealba, L. C., & Alvarez-Buylla, A. (2019). Development of ependymal and postnatal neural stem cells and their origin from a common embryonic progenitor. *Cell Reports*, *27*(2), 429–441 e3.

Rice, M. E. (2000). Ascorbate regulation and its neuroprotective role in the brain. *Trends in Neurosciences*, *23*(5), 209–216.

Salazar, K., Cerda, G., Martínez, F., Sarmiento, J. M., González, C., Rodríguez, F., García-Robles, M., Tapia, J. C., Cifuentes, M., & Nualart, F. (2014). SVCT2 transporter expression is post-natally induced in cortical neurons and its function is regulated by its short isoform. *Journal of Neurochemistry*, *130*(5), 693–706.

Salazar, K., Espinoza, F., Cerda-Gallardo, G., Ferrada, L., Magdalena, R., Ramírez, E., Ulloa, V., Saldivia, N., Troncoso, N., Oviedo, M. J., Barahona, M. J., Martínez, F., & Nualart, F. (2021). SVCT2 overexpression and ascorbic acid uptake increase cortical neuron differentiation, which is dependent on vitamin C recycling between neurons and astrocytes. *Antioxidants (Basel)*, *10*(9), 1413–1428.

Salazar, K., Jara, N., Ramírez, E., de Lima, I., Smith-Ghigliotto, J., Muñoz, V., Ferrada, L., & Nualart, F. (2023). Role of vitamin C and SVCT2 in neurogenesis. *Frontiers in Neuroscience*, *17*, 1155758.

Salazar, K., Martínez, F., Pérez-Martín, M., Cifuentes, M., Trigueros, L., Ferrada, L., Espinoza, F., Saldivia, N., Bertinat, R., Forman, K., Oviedo, M. J., López-Gambero, A. J., Bonansco, C., Bongarzone, E. R., & Nualart, F. (2017). SVCT2 expression and function in reactive astrocytes is a common event in different brain pathologies. *Molecular Neurobiology*, *55*, 5439–5452.

Salazar, K., Martínez, M., Ulloa, V., Bertinat, R., Martínez, F., Jara, N., Espinoza, F., Bongarzone, E. R., & Nualart, F. (2016). SVCT2 overexpression

10981136, 0, Downloaded from https://onlinelibrary.wiley.com/doi/10.1002/glia.24498 by Cbua-Consorcio De Bibliotecas, Wiley Online Library on [26/01/2024]. See the Terms and Conditions (https://onlinelibrary.wiley.com/terms-and-conditions) on Wiley Online Library for rules of use; OA articles are governed by the applicable Creative Commons License

in neuroblastoma cells induces cellular branching that is associated with ERK signaling. *Molecular Neurobiology*, *53*(10), 6668–6679.

Sanai, N., Nguyen, T., Ihrie, R. A., Mirzadeh, Z., Tsai, H. H., Wong, M., Gupta, N., Berger, M. S., Huang, E., Garcia-Verdugo, J. M., Rowitch, D. H., & Alvarez-Buylla, A. (2011). Corridors of migrating neurons in the human brain and their decline during infancy. *Nature*, *478*(7369), 382–386.

Sarbassov, D. D., Guertin, D. A., Ali, S. M., & Sabatini, D. M. (2005). Phosphorylation and regulation of Akt/PKB by the rictor-mTOR complex. *Science*, *307*(5712), 1098–1101.

Saxton, R. A., & Sabatini, D. M. (2017). mTOR signaling in growth, metabolism, and disease. *Cell*, *169*(2), 361–371.

Semprich, C. I., Davidson, L., Amorim Torres, A., Patel, H., Briscoe, J., Metzis, V., & Storey, K. G. (2022). ERK1/2 signalling dynamics promote neural differentiation by regulating chromatin accessibility and the polycomb repressive complex. *PLoS Biology*, *20*(12), e3000221.

Shin, D. M., Ahn, J. I., Lee, K. H., Lee, Y. S., & Lee, Y. S. (2004). Ascorbic acid responsive genes during neuronal differentiation of embryonic stem cells. *Neuroreport*, *15*(12), 1959–1963.

Siegenthaler, J. A., Ashique, A. M., Zarbalis, K., Patterson, K. P., Hecht, J. H., Kane, M. A., Folias, A. E., Choe, Y., May, S. R., Kume, T., Napoli, J. L., Peterson, A. S., & Pleasure, S. J. (2009). Retinoic acid from the meninges regulates cortical neuron generation. *Cell*, *139*(3), 597–609.

Silva-Alvarez, C., Salazar, K., Cisternas, P., Martínez, F., Liour, S., Jara, N., Bertinat, R., & Nualart, F. (2016). Apical polarization of SVCT2 in apical radial glial cells and progenitors during brain development. *Molecular Neurobiology*, *54*, 5449–5467.

Sinor, A. D., & Lillien, L. (2004). Akt-1 expression level regulates CNS precursors. *The Journal of Neuroscience*, *24*(39), 8531–8541.

Sotiriou, S., Gispert, S., Cheng, J., Wang, Y., Chen, A., Hoogstraten-Miller, S., Miller, G. F., Kwon, O., Levine, M., Guttentag, S. H., & Nussbaum, R. L. (2002). Ascorbic-acid transporter Slc23a1 is essential for vitamin C transport into the brain and for perinatal survival. *Nature Medicine*, *8*(5), 514–517.

Spear, P. C., & Erickson, C. A. (2012). Interkinetic nuclear migration: A mysterious process in search of a function. *Development, Growth & Differentiation*, *54*(3), 306–316.

Spector, R., & Lorenzo, A. V. (1974). Specificity of ascorbic acid transport system of the central nervous system. *The American Journal of Physiology*, *226*(6), 1468–1473.

Stadtfeld, M., Apostolou, E., Ferrari, F., Choi, J., Walsh, R. M., Chen, T., Ooi, S. S. K., Kim, S. Y., Bestor, T. H., Shioda, T., Park, P. J., & Hochedlinger, K. (2012). Ascorbic acid prevents loss of Dlk1-Dio3 imprinting and facilitates generation of all-iPS cell mice from terminally differentiated B cells. *Nature Genetics*, *44*(4), 398–405. S1–S2.

Su, X., Shen, Z., Yang, Q., Sui, F., Pu, J., Ma, J., Ma, S., Yao, D., Ji, M., & Hou, P. (2019). Vitamin C kills thyroid cancer cells through ROS-dependent inhibition of MAPK/ERK and PI3K/AKT pathways via distinct mechanisms. *Theranostics*, *9*(15), 4461–4473.

Temple, S. (2001). The development of neural stem cells. *Nature*, *414*(6859), 112–117.

Tong, C. K., Han, Y. G., Shah, J. K., Obernier, K., Guinto, C. D., & Alvarez-Buylla, A. (2014). Primary cilia are required in a unique subpopulation of neural progenitors. *Proceedings of the National Academy of Sciences of the United States of America*, *111*(34), 12438–12443.

Tramontin, A. D., García-Verdugo, J. M., Lim, D. A., & Alvarez-Buylla, A. (2003). Postnatal development of radial glia and the ventricular zone (VZ): A continuum of the neural stem cell compartment. *Cerebral Cortex*, *13*(6), 580–587.

Tsukaguchi, H., Tokui, T., Mackenzie, B., Berger, U. V., Chen, X. Z., Wang, Y., Brubaker, R. F., & Hediger, M. A. (1999). A family of mammalian Na+−dependent L-ascorbic acid transporters. *Nature*, *399*(6731), 70–75.

Ulloa, V., García-Robles, M., Martínez, F., Salazar, K., Reinicke, K., Pérez, F., Godoy, D. F., Godoy, A. S., & Nualart, F. (2013). Human choroid plexus papilloma cells efficiently transport glucose and vitamin C. *Journal of Neurochemistry*, *127*(3), 403–414.

Ulloa, V., Saldivia, N., Ferrada, L., Salazar, K., Martínez, F., Silva-Alvarez, C., Magdalena, R., Oviedo, M. J., Montecinos, H., Torres-Vergara, P., Cifuentes, M., & Nualart, F. (2019). Basal sodium-dependent vitamin C transporter 2 polarization in choroid plexus explant cells in normal or scorbutic conditions. *Scientific Reports*, *9*(1), 14422.

Villalba, A., Gotz, M., & Borrell, V. (2021). The regulation of cortical neurogenesis. *Current Topics in Developmental Biology*, *142*, 1–66.

Voigt, T. (1989). Development of glial cells in the cerebral wall of ferrets: Direct tracing of their transformation from radial glia into astrocytes. *The Journal of Comparative Neurology*, *289*(1), 74–88.

Wang, B., Gao, Y., Xiao, Z., Chen, B., Han, J., Zhang, J., Wang, X., & Dai, J. (2009). Erk1/2 promotes proliferation and inhibits neuronal differentiation of neural stem cells. *Neuroscience Letters*, *461*(3), 252–257.

Wang, S., Liang, Q., Qiao, H., Li, H., Shen, T., Ji, F., & Jiao, J. (2016). DISC1 regulates astrogenesis in the embryonic brain via modulation of RAS/-MEK/ERK signaling through RASSF7. *Development*, *143*(15), 2732–2740.

Wang, T., Chen, K., Zeng, X., Yang, J., Wu, Y., Shi, X., Qin, B., Zeng, L., Esteban, M. A., Pan, G., & Pei, D. (2011). The histone demethylases Jhdm1a/1b enhance somatic cell reprogramming in a vitamin-C-dependent manner. *Cell Stem Cell*, *9*(6), 575–587.

Wu, H., Wu, Y., Ai, Z., Yang, L., Gao, Y., du, J., Guo, Z., & Zhang, Y. (2014). Vitamin C enhances Nanog expression via activation of the JAK/STAT signaling pathway. *Stem Cells*, *32*(1), 166–176.

Yan, J., Studer, L., & McKay, R. D. (2001). Ascorbic acid increases the yield of dopaminergic neurons derived from basic fibroblast growth factor expanded mesencephalic precursors. *Journal of Neurochemistry*, *76*(1), 307–311.

Zhang, J., Shemezis, J. R., McQuinn, E. R., Wang, J., Sverdlov, M., & Chenn, A. (2013). AKT activation by N-cadherin regulates beta-catenin signaling and neuronal differentiation during cortical development. *Neural Development*, *8*, 7.

Zhang, S., & Cui, W. (2014). Sox2, a key factor in the regulation of pluripotency and neural differentiation. *World Journal of Stem Cells*, *6*(3), 305–311.

SUPPORTING INFORMATION

Additional supporting information can be found online in the Supporting Information section at the end of this article.

How to cite this article: Saldivia, N., Salazar, K., Cifuentes, M., Espinoza, F., Harrison, F. E., & Nualart, F. (2024). Ascorbic acid and its transporter SVCT2, affect radial glia cells differentiation in postnatal stages. *Glia*, 1–20. https://doi.org/10.1002/glia.24498

10981136, 0, Downloaded from https://onlinelibrary.wiley.com/doi/10.1002/glia.24498 by Chun-Consorcio De Bibliotecas, Wiley Online Library on [26/01/2024]. See the Terms and Conditions (https://onlinelibrary.wiley.com/terms-and-conditions) on Wiley Online Library for rules of use; OA articles are governed by the applicable Creative Commons License